Torque Control Strategies for AWD Electric vehicles

by

Christopher J. Mendes

A thesis
presented to the University of Waterloo
in fulfillment of the
thesis requirement for the degree of
Master of Applied Science
in
Mechanical Engineering

Waterloo, Ontario, Canada, 2006

Author's Declaration

I hereby declare that I am the sole author of this thesis. This is a true copy of the thesis, including any required final revisions, as accepted by my examiners.

I understand that my thesis may be made electronically available to the public.

Abstract

There is a fundamental shift occurring in the design of passenger vehicles for North American markets. While for decades automotive manufacturers have relied on internal combustion engines burning fossil fuels, the early 21st century has seen a departure from conventional thinking about powertrain design towards two new design paradigms: hybrid electric vehicles (HEVs), and fuel cell vehicles (FCVs).

Hybrid electric vehicles incorporate a high power electric motor and an electrical storage system which are used for motive power in addition to their conventional internal combustion engine (ICE). Fuel cell vehicles use a stack of individual cells to produce electric power which is then used in an electric motor to move the vehicle. They are generally fueled by a stream of high purity hydrogen, and produce only water as an emission. Both vehicle types use electric motors as an integral component in their configuration.

The objective for this thesis is to propose a control strategy for the traction motors of a hybrid or electric vehicle. In particular, it addresses the question of how to split torque between two onboard electric motors while considering the efficiency, stability, and traction of the vehicle. This work is based upon two hybrid vehicles: a Chevrolet Equinox converted to a Fuel Cell HEV, and a Chrysler Pacifica converted to an internal combustion engine HEV.

A torque control strategy is recommended that focuses on improved efficiency while addressing vehicle stability, and traction control. The strategy also incorporates powertrain component protection. Simulations indicate that the manner in which torque is split between the motors can have a large impact on the total efficiency of the powertrain; greater than 7% improvement fuel economy is projected by using an intelligent torque control system over a

FTP-75 drive cycle. It is recommended that this work be extended to incorporate regenerative braking and a more thorough analysis of vehicle stability and drivability.

Acknowledgements

I would like to thank my supervisors, Dr. Roydon Fraser, and Dr. Steve Lambert, for their patience, insights, and sure-handed guidance during my graduate studies and during the writing of this thesis.

I would also like to acknowledge the support and funding of the Auto21 Network of Centers of Excellence, in addition to the contributions of the researchers and HQP at the University of Windsor and University of British Columbia.

I would also like to express my gratitude and admiration for my fellow teammates from the Alternative Fuels Team for their daily (and nightly) demonstrations of their commitment to the project. It has been an absolute delight to be able to work and grow surrounded by such talented people.

Lastly, I would like to thank my family and parents for their unending support for my educational aspirations, and indeed encouraging me to chase all my goals.

Dedication

This thesis is dedicated to my friend Michelle, who continues to daily teach me the difference between knowledge and wisdom.

Table of Contents

List of Figures

List of Tables

Chapter 1
Introduction

Environmental, political, and economic pressure has been steadily increasing since the late 1990's on automotive manufacturers to produce vehicles that consume less fuel and produce less harmful emissions. Most manufacturers in the passenger vehicle market seem to be turning towards electrification of the powertrain to achieve these goals, either using a hybrid approach, gasoline engine and electric motors; or a fully electric approach, electrochemical storage, or fuel cell-based[1].

Hybrid vehicles are generally defined as containing a mechanism for temporary storage of energy for motive use, as well as a separate method for converting the primary energy source to mechanical energy. This could be instantiated a number of different ways, with the type of hybrid generally specified by the energy storage mechanism used. Battery systems, electrolytic capacitors, compressed air, and hydraulic reservoirs are some of the technologies that have been demonstrated in passenger vehicles. The benefits of hybridization, regardless of energy storage type are:

- the ability to reduce engine use under transient-conditions where efficiency is lower or emissions production is higher, while still delivering the same amount of torque to meet driver requests
- the ability to recapture some portion of the vehicle kinetic energy while braking,
- and the ability to downsize the installed engine.

The technology that has been best characterized and has been deployed for a number of years in the marketplace is electrochemical batteries for storage and using electric motors to produce motive torque. This technology has a number of inherent advantages over other storage mechanisms, including an appropriate ratio of power/energy capability, high efficiency, and low weight.

As of 2006, hybrid technology is still in the growth stage, with few production models being offered. At the end of 2006 there were 6 hybrid cars, 5 hybrid SUV's, and two mild-hybrid pickup trucks available in the North American markets[2]. As hybrid technology advances it will be applied to a greater breadth of vehicles, some of which will presumably be 4-wheel drive vehicles. Of the 13 vehicles currently offered, two of them (the Toyota highlander and the Lexus RX 400h) have 4-wheel drive that is achieved via separate electric motors driving the front and rear wheels.

Hybrids are not restricted to internal combustion engines. Fuel cells too can be used as the primary power producer. The most common type of fuel cell envisioned, and invested in for vehicular applications, is the 'proton exchange membrane' (PEM) technology. All fuel cells, including PEM types, produce current by routing the electrons involved in the reaction through the devices that need electrical power before consuming them to complete the reaction[3]. These vehicles are even more suited for electrical hybridization than internal combustion engines: The fuel cell is already producing electrical power that can be interfaced with a high efficiency DC/DC voltage converter, to a chemical or electrolytic capacitor storage mechanism. This vehicle will assuredly use electric motors to produce torque. For example, GM recently showcased their manufacturable fuel cell vehicle named the 'Sequel'. This vehicle incorporates three electric motors: one single motor driving the front axle, and two hub motors propelling the rear axle[4].

The trends in electrical hybridization and AWD as illustrated by GM's Sequel offer significant opportunities for innovative control strategies to improve vehicle dynamic behavior and overall system efficiency. Much effort has been expended on electronic stability programs[5] and efficient control of hybrid systems[6]. This thesis will focus on the potential efficiency improvements through power management between the front and rear axles.

1.1 Project Objective

This project's objective is to generate an efficiency improving torque control strategy for a vehicle that is driven by two electric axle-motors. The work focuses around the control of two vehicles that were (in-part) engineered at the University of Waterloo: a 2004 Chrysler Pacifica, which was converted to an Ultracapacitor-based hybrid electric vehicle (HEV), retaining the original internal combustion engine, and a 2005 Chevrolet Equinox, which was converted to a fuel cell hybrid electric vehicle (FCHEV)[7]. These vehicles had different levels of modifications: the Equinox's entire powertrain and driveline were replaced with two electric axle-motors; the Pacifica's propeller shaft was replaced with two motors, one driving the transfer case and one driving the rear differential. Both vehicles required a control strategy. The specific implementation must consider: drivability, stability, traction control, and efficiency. It should be noted that although this work focuses on hybrid vehicles, it applies equally to Battery-powered electric vehicles (BEV).

The Chevrolet Equinox fuel cell powertrain was designed to provide the same performance characteristics as the original vehicle. Figure 1-1 shows the powertrain configuration used to achieve this goal. Two identical motors were used to deliver mechanical power to the vehicle. The vehicle was University of Waterloo's entry into the ChallengeX competition[8]; a competition involving 17 universities across North America who compete to produce the most environmentally-friendly, but still market-ready vehicle. The competition is headline sponsored by GM and the United States Department of Energy. The University of Waterloo's entry was designed and built by the Alternative Fuels Team[9], a cross-disciplinary engineering student team. The author played a role in this team as technical director from 2004-2005 and co-captain from 2005-2006.

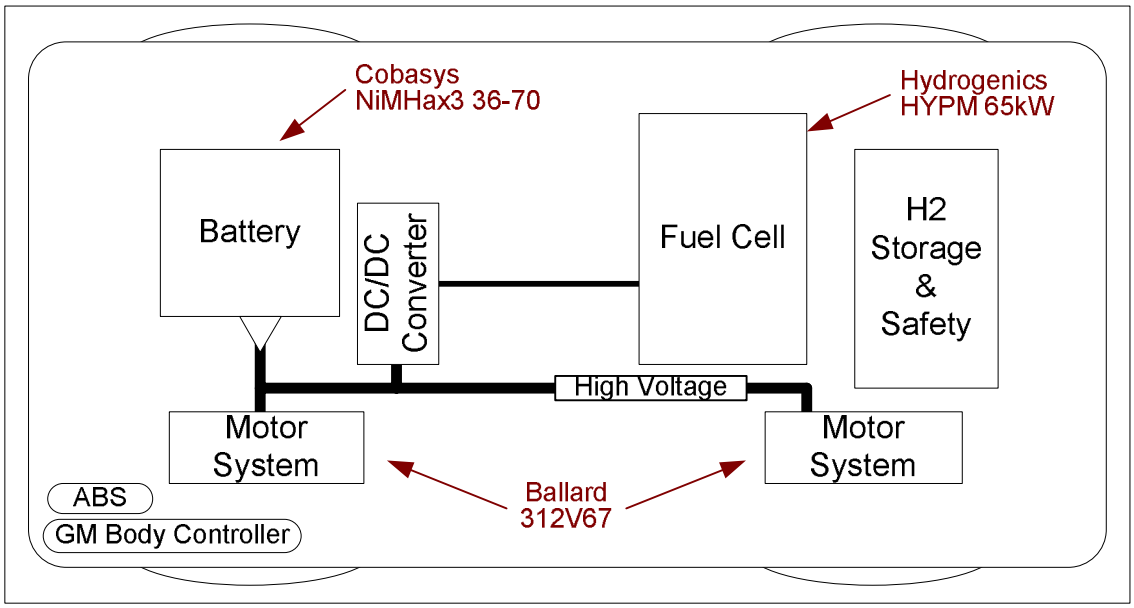

Figure 1-1: The Equinox Powertrain Schematic

The Chrysler Pacifica modifications were designed in order to investigate and benchmark regenerative braking concepts. The vehicle schematic can be seen in figure 1-2. It too uses two motors, a Ballard 312V67 system on the front, and a second, smaller AC induction motor on the rear.

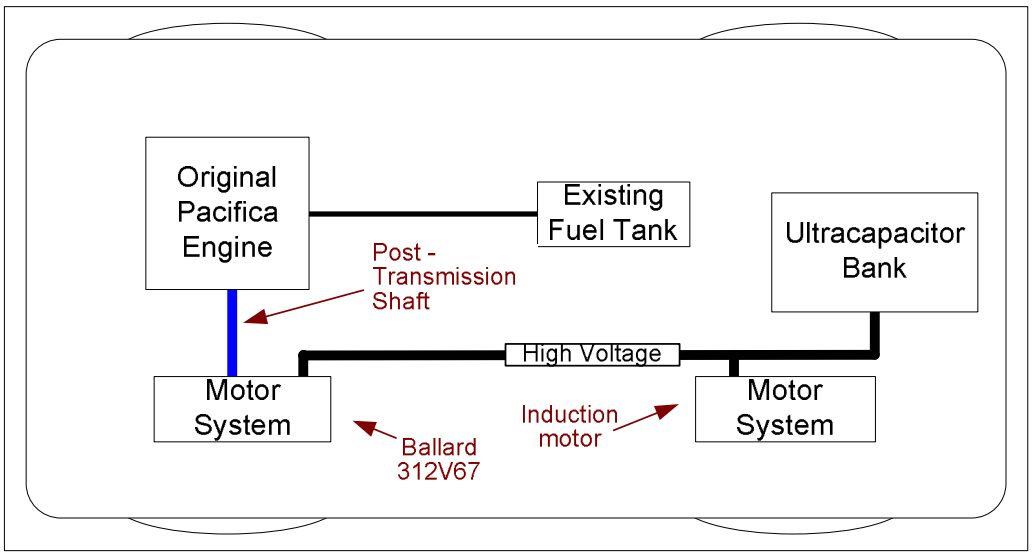

Figure 1-2: Chrysler Pacifica Powertrain Schematic

The Chrysler Pacifica project was multi-stage, with the functionality and system complexity of the system increasing with each stage. The first stage included only the front motor and the

ultracapacitors, the second stage includes the second motor on the rear axle, and the third stage supplemented the Ultracapacitor storage with a battery pack (not shown)[10].

1.1.1 Focus and Scope of Work

This work is predicated upon the expectation that some efficiency gain is possible by the intelligent sharing of torque between motors due to the non-linear efficiency maps of the motor technology. In order to realize this gain, there is a preliminary need to create a framework and methodology to address the issue of torque control. This torque control strategy must address the issue of how much torque should be available to the driver and how that torque will be rationed by the throttle. It must consider the protection of the powertrain components, the stability of the vehicle, the drive quality of the vehicle, and, finally, the efficiency of the torque production.

The specific objectives for this project are as follows:

- to provide a control framework which is flexible enough to allow the evaluation of alternative strategies, and
- to provide a torque split map that will optimize overall motor efficiency.

An additional goal for the Equinox, due to its fuel cell configuration, is to provide strategies that will protect the upstream powertrain from harmful transient and steady-state conditions.

Emphasis has been placed on the development of a system for the Equinox. The Equinox torque control framework will be presented with the balance of the powertrain controls. The Pacifica was used to demonstrate the generality of the approach; however, the further integration of the efficiency mapping into the Pacifica control code is outside the scope of this thesis.

Chapter two of this thesis starts with an overview of the marketplace context, providing the motivation and justification for this work in light of possible future pathways of vehicle technology. Chapter three reviews why hybrid technology is increasingly relevant today, and includes background information on the different types, how they work and why they are effective. It also explores the impact of drive cycles on these vehicles, and how accurate drive cycles truly are today. Chapter four covers background information on fuel cell vehicles and the process of designing them. Chapter five provides background on motor technology, its benefits and drawbacks, how torque control is implemented, and the mechanisms for losses. Chapter six delves into the problem of torque control, proposes a controls framework, and provides a set of codified solutions to fulfill this framework. The vehicle models used to generate and tune the solutions are presented, along with the results from these simulations. Finally, recommendations and conclusions are presented in Chapter seven.

Chapter 2

The Future of the Automobile

This section establishes the motivation for examining the technical problems surrounding electric vehicles. It covers the economic, environmental, and political forces acting to move powertrain technology towards the hybridization of internal combustion engines, and eventually to the hybridized fuel cells topology.

2.1 Marketplace Overview

The impetus for this work comes from the increasing development and deployment of electric powertrains for passenger vehicles. There are two types of electric powertrains on the market currently: fully-electric, which are currently relegated to niche markets, such as airport ground support vehicles or golf carts, and hybrid vehicles, which have begun to make inroads into the passenger vehicle market. Due to the rapidly increasing cost of energy, which is changing vehicle lifecycle economics, it is becoming increasingly clear the automotive market is in transition to more efficient technology. This is driving the initial cost of vehicles up in order to reduce the total cost of vehicle ownership to both the owner and the environment.

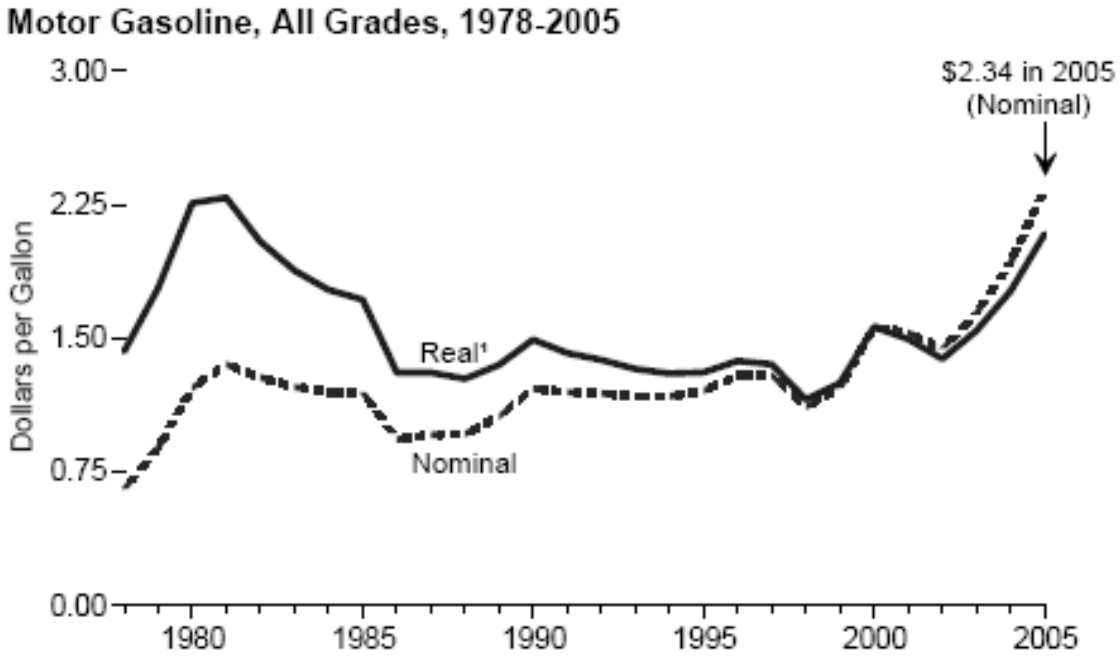

Figure 2-1: The real and inflation-adjusted (2000 dollars) average U.S. price of engine gasoline from 1978-2005[11].

As can be seen from Figure 2-1, the average price of retail gasoline has been in rapid growth since its low in 1998 and, at the end of 2005 was close to the all time highs of 1980. There are many possible reasons for the increase in oil and gasoline prices: regional instability, the inability of oil production to match economic growth, and environmental and technical problems. Also possible is that lack of new oil field discoveries are increasing dependence on existing wells. If this is the case, and the world is experiencing a run-up to peak oil production[12], then the automotive industry will truly be entering a period of fundamental change, during which it will become economically advantageous, and eventually a requisite, to produce cars that use alternative energy sources.

The pathway to a non-petroleum based transportation infrastructure is seen by many experts to be one of internal combustion engine (ICE)-based hybrid powertrains in the mid-term, and hydrogen-based power-trains in the long term – see figure 2-2. One key technology in both these cases is medium voltage (300-500VDC) electric motors that either complement the ICE technology, in the case of hybrids, or simply replace it, as in the case of electric vehicles (EV).

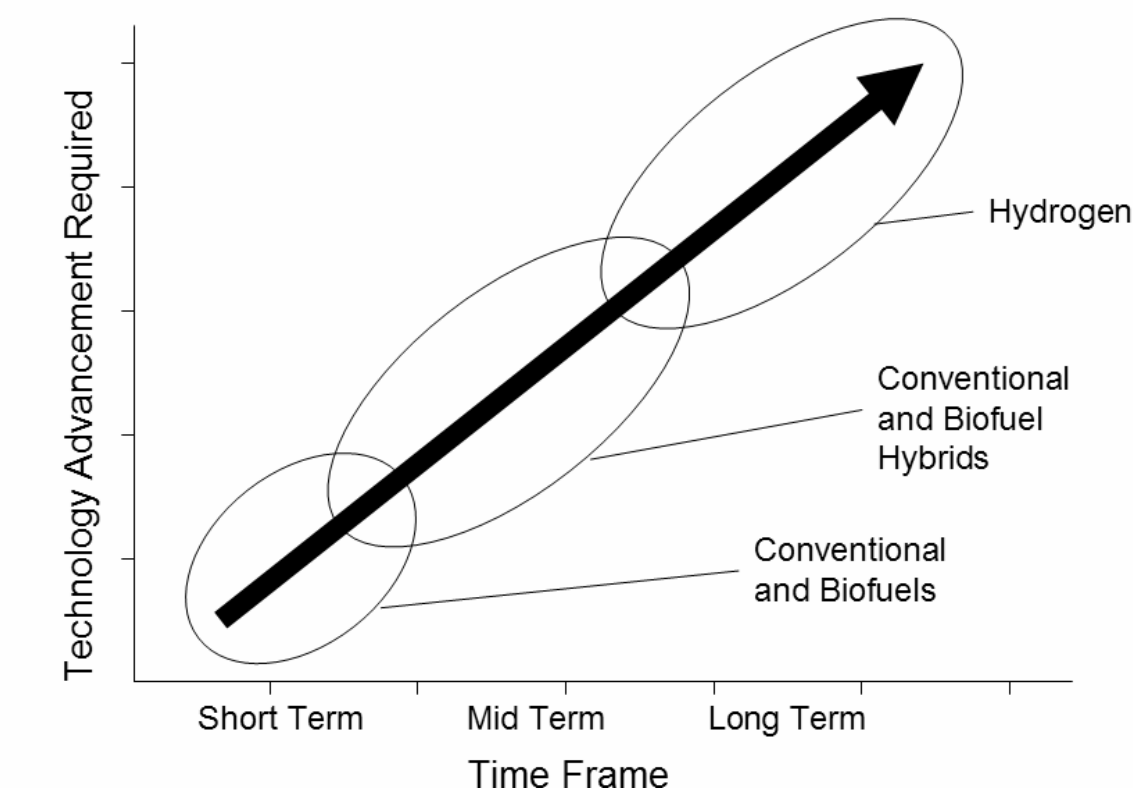

Figure 2-2: The automotive technological pathway envisioned by a number of automotive manufacturers[13].

Using hydrogen as an energy carrier is currently the favored *long-term* solution by both government and industry in North America to reduce dependence on petroleum, cut emissions, and provide a clear path to a sustainable energy economy – one in which the energy used is based on renewable resources[1]. However, there are a number of other potential technologies that may fill niche transportation roles: Compressed air, chemical batteries, and ultra-capacitors are all candidates to become a viable energy storage mechanism for automotive. Hydrogen fuel cells have the edge on these other technologies by combining high power density with the potential for high energy storage, and the potential for costing at the level of ICE technology along with the reliability and durability necessary for automotive applications[14].

Regardless of the onboard storage technology, the presence of electricity in the future of automotive technology is generally taken for granted. Electrification offers several benefits, including an unparalleled number of production paths, pre-existing infrastructure, a multitude of potential storage options, and reduced dispersed-environmental, regional, and political stress.

Chapter 3

Hybrid Vehicle Overview

Hybrid vehicles have quickly become a burgeoning force in the North American market, ostensibly driven by increased consumer sensitivity to fuel prices and environmental considerations. Hybrid technology creates benefits for consumers in both areas by decreasing fuel consumption compared to conventional vehicles.

3.1 Hybrid Electric Vehicles (HEVs)

HEVs first started appearing on North American roads in 1999, and have steadily grown in diversity and numbers[15]. Surprisingly, a significant part of this sales growth has little to do with reduced fuel costs, or protecting the environment, but rather perceived symbolism that these vehicles project. In fact, Heffner, et al.[16] concludes that a significant number of hybrid buyers have misunderstandings about basic environmental problems, and illustrates owner's deficient understanding of the environmental impact of their HEV's. Regardless of this fact, there are real, tangible benefits to hybrid technology as fuel costs rise, and environmental degradation becomes an increasingly more pressing issue. A 2004 paper from the Princeton Environmental Institute[17] presents comprehensive societal lifecycle costs (LCC) of different automotive technology in a bid to predict the appropriate pathway for automotive investment. It clearly denotes HEV's as the near term solution to reducing automotive LCCs, and fuel cell vehicles as the eventual successor, endorsing the technological pathway illustrated in figure 2-2. Both these vehicles reduce the LCC of greenhouse gases (GHG), air pollution, and oil supply insecurity; this pathway manages to have only a single fuelling infrastructure change.

3.2 Hybrid Electric Vehicle Technology

Hybrid vehicles require a mechanism to store energy produced from the prime energy converter or from recovery of the vehicle's kinetic energy. This energy storage mechanism could be a battery, a solid state storage system such as a capacitor, an electro-mechanical system such as a flywheel, or a fully mechanical system such as a hydraulic accumulator[10].

Hybrid electric vehicles can improve fuel economy via some or all of the following mechanisms[10]:

- Elimination of engine idling
- All electric mode in low power, high transient environments
- Regenerative braking to capture kinetic energy
- Power splitting in order to improve overall efficiency

Note that the hybrid vehicle's ability to improve overall fuel consumption is fully dependant on how the vehicle is driven and is best for transient driving conditions. Certain vehicle-specific driving patterns lend themselves well to hybridization, such as city buses, urban delivery trucks, and garbage trucks. Vehicles that spend a significant time at constant speed, such as Class 8 tractor-trailers, will not benefit from hybridization to the same degree[10].

There are many permutations of hybrid vehicles configurations, which can be classified as parallel, series, and parallel-series. These configurations encompass hybrid fuel cell vehicles (FCVs) and ICE-HEV's.

3.2.1 Parallel Hybrids

In the parallel configuration, shown in figure 3-1[18], the torque of the motor and the engine can be summed through a gearbox (or through the road) to move the vehicle. In addition, the motor can act as a generator in order to charge the battery, absorbing energy from either the engine, or the vehicle's kinetic motion. One advantage of this configuration is that the engine and motor can be sized smaller than the peak loads expected, reducing weight and cost. One drawback is that the engine speed and motor speeds are directly linked through the gearbox, limiting the ability for the system to change the operating points of the powertrain in order to boost efficiency.

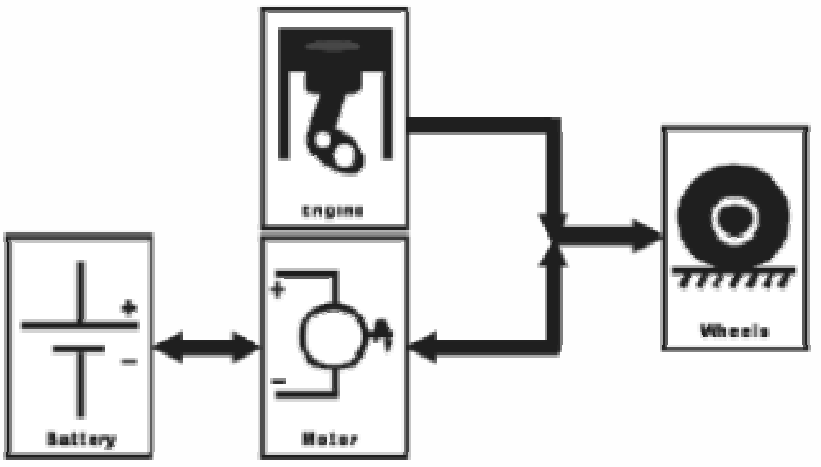

Figure 3-1: Example parallel hybrid configuration

3.2.2 Series Hybrid

The series configuration shown in figure 3-2[18] is rarely seen in passenger vehicles, but can be seen in locomotive or marine applications, where the magnitude of the torques and loads preclude the use of conventional clutches. The main drawback of this configuration is that since all wheel torque must come from the tractive motor, this motor must be sized for the peak loads required. This makes this configuration more expensive than the parallel configuration. The benefit of this system is that the engine/generator couple can be run at their most efficient point more often, as there is a decoupling effect due to the genset; this enables large gains, since the engine is generally much less efficient than the other components – having the combustion engine run at peak efficiency can yield large benefits.

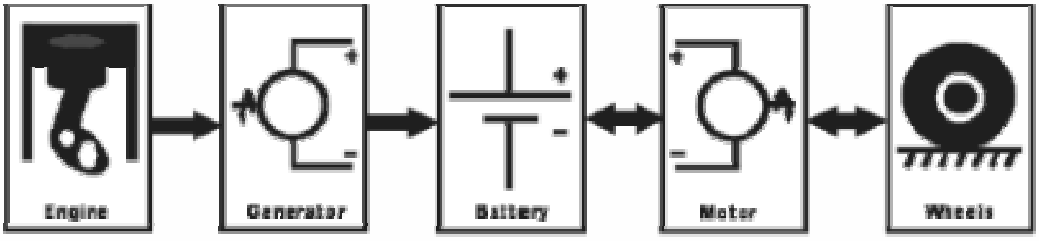

Figure 3-2: The series hybrid configuration

3.2.3 Parallel-Series Hybrid

The parallel-series hybrid combines the best of the parallel and series configurations, as can be seen in figure 3-3[18]. This configuration allows the vehicle to run in a series mode by disconnecting the engine from the wheels, and using one of the motors to drive the vehicle. It can also work as a parallel configuration, with both motors and the engine combining to deliver torque to the wheels. It can be cheaper than the series configuration since the motors can be downsized, and allows an additional degree of freedom in the control strategy, since the engine can often be run at its most efficient point. The additional degree of freedom created by this configuration (over the series or parallel configuration) mandates a higher degree of control complexity[6].

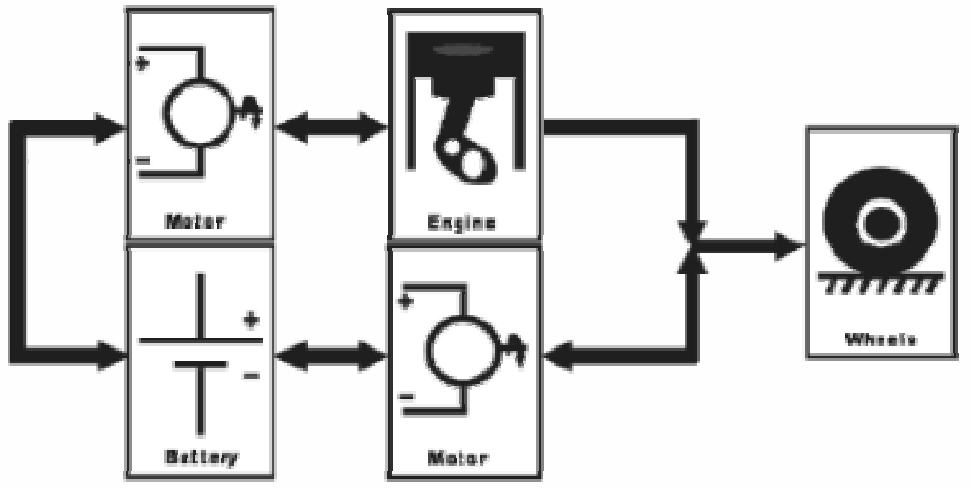

Figure 3-3: The parallel-series hybrid configuration

Both the Equinox and the Pacifica are parallel configurations; the Pacifica is a parallel HEV, where the mechanical shaft power is summed, and the Equinox is a parallel FCHEV, where the electrical power is summed.

3.3 Drive cycles

One of the most challenging aspects of vehicle design involves creating vehicles that satisfy a variety of customers who expect a wide variety of performance and utility levels from their vehicles. As the energy efficiency of automobiles becomes more important to vehicle designers, the need for valid data on driving habits and patterns grows accordingly.

In order to consistently evaluate vehicles according to some predefined set of metrics, designers (and vehicle evaluators) need a representative drive cycle: a time-speed curve that captures the manner in which the vehicles will be used. This data allows power-train engineers to optimize vehicles for the customers, and it allows vehicle evaluators a consistent manner in which to test and grade vehicles. The most commonly used drive cycle in North America is the Federal Test Procedure 75 (FTP-75) cycle[19].

3.3.1 FTP drive cycle history

The Federal Test Procedure (FTP-75)[19] drive cycle was borne out of the work done by employees of the Vehicle Pollution Laboratory in California. They drove a test vehicle on their actual home-to-work route and recorded the manifold pressure and engine rpm. They then found a single route, through central Los Angeles, that statistically matched the data collected from multiple home-to-work trials. They named this the LA4 cycle. Soon afterward, the EPA's West

Coast Laboratory became interested in developing a federal drive cycle and generated time-speed data for the LA4 route. Several modifications were made to this cycle, including shortening it to what was then believed to be the average Los Angeles trip distance (7.46 miles), and limiting the minimum and maximum accelerations to ±1.47 m/s^2, what was then the limit of the belt-driven dynamometers in use. In 1975, the drive cycle was extended; repeating the first 505 seconds of the cycle after a period of vehicle inactivity allowed the characterization of vehicle emissions while the vehicle was warm. This cycle was named the FTP-75 cycle and can been seen in figure 3-4[19]. Figure 3-5[19] shows the speed vs. acceleration scatter plot of the FTP-75 cycle.

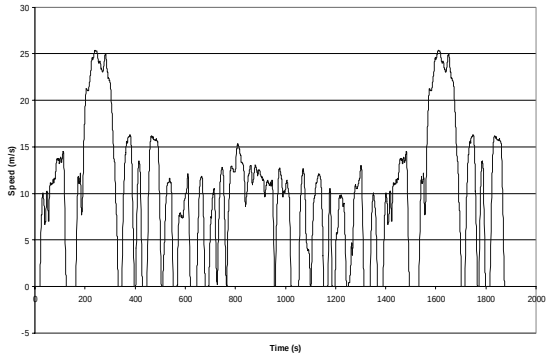

Figure 3-4: The vehicle speed vs. time profile of the FTP-75 drive cycle

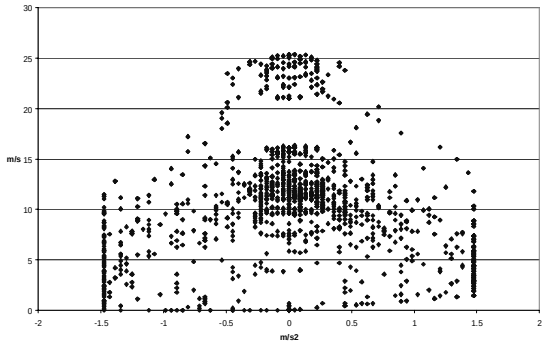

Figure 3-5: The speed vs. acceleration scatter plot for the FTP-75 cycle

3.3.2 FTP comparison to present-day driving patterns

Unfortunately, there is little available data on present day real-world driving cycles. One report which does detail a significant amount of data was generated by the United States Environmental Protection Agency (the EPA)[19] in 1993. This report compared and contrasted the FTP cycle to real-world driving data produced from four experiments in Spokane, Baltimore, Atlanta, and Los Angeles. These experiments consisted of a combination of instrumenting vehicles to record time-speed traces (among other things), and a chase-vehicle mounted laser to record time-speed traces of randomly chosen drivers.

The conclusions of the study focused around the impact of the cycles on emissions, and suggested developing cycles that represented the greater variation present in real-world driving. Table 3-2 shows the results of the study: the FTP cycle seems to present a ‘moderate’ fit to the real world data; average speeds are slightly lower, but the acceleration distributions and power averages of the FTP-75 are realistic. Of interest is the significant difference between the FTP cycle and the minimum and maximum of all metrics. There is extremely aggressive braking, accelerating, and power metrics found in the experimental trials.

Table 3-1: A comparison of speed, acceleration, and power data from the EPA real-world drive cycle studies and the FTP cycle

		Baltimore	Spokane	Atlanta	Los Angeles	FTP
Speed						
m/s	**Average**	10.95	10.39	12.87	12.67	**8.76**
	Max	42.22	34.66	43.12	35.89	**25.34**
	Std Dev	9.17	7.92	10.10	9.01	**6.57**
Accel						
m/s^2	**Min**	-8.71	-6.91	8.32	-6.70	**-1.48**
	Max	6.79	7.13	7.46	4.65	**1.48**
	Std Dev	0.67	0.65	0.68	0.78	**0.63**
Power						
m^2/s^3	**Average**	9.19	8.02	10.33	11.78	**7.71**
	Max	111.42	134.31	144.47	153.65	**38.33**
	Std Dev	8.58	8.16	9.61	9.81	**6.34**

In order to process this data to determine the operational points of the motor, one would need to generate the vehicle speed-acceleration joint distribution. Unfortunately, this distribution is not retrievable from the above metrics – the only hint about this distribution comes from the 'power' metric, which is defined in the study as:

$$Power = 2 \times Speed \times Acceleration \quad \textbf{(1)}$$

The power distribution gives an indication of the power that the drive-train is producing, but has confounded the speed and acceleration, preventing the deduction of the speed-acceleration joint distribution. This speed-acceleration joint distribution is needed to perform simulations to attempt to quantify the efficiency of the vehicle.

There is an important, additional factor that is unaccounted for in both the FTP cycle, and the test data from Spokane, Baltimore, Atlanta, and L.A.: road grade. Unfortunately road grade statistics are not well known – the data shown in table 3-3 was generated from the Passenger Car Fuel Economy study performed by the EPA in 1980[20]. Clearly, a large proportion of driving time is performed on non-flat roads. The impact of nation-wide road grades on fuel economy is unknown at this point, and warrants further research.

Table 3-2: Road gradient (%) vs. percentage of vehicle miles traveled (VMT) nationwide (U.S.)

Road Gradient (%)	Percent of VMT
<0.5	35
0.5 - 1	20
1 - 2	15
2 - 3	10
3 - 4	8
4 - 5	6
5 - 6	4
>6	2

3.4 Hybrid Control Strategies

While the hybrid hardware in these vehicles are the enablers that produce the potential for the fuel-saving benefits, an appropriate control strategy must be employed in order to take full advantage of the hardware, and to derive maximum efficiency and power. These control strategies sit highest in the hierarchy of onboard vehicle controllers, and determine the operational mode of the vehicle (electric, conventional, or hybrid), and the instantaneous split of power between components. There are a vast number of academic papers exploring hybrid control strategies, most dealing with the power split between motors and engines, in ICE-HEVs, and between fuel cell and batteries, in fuel cell vehicles[6,21]. One subset of a comprehensive hybrid control strategy, torque control, will be presented in this document.

Chapter 4
Fuel Cell Vehicle Overview

The introduction of the fuel cell vehicle into the marketplace will mark a truly new paradigm in the delivery and consumption of energy for personal transportation; energy will no longer need to be extracted from non-renewable ground reserves. Energy can be derived from fully renewable energy sources, thus allowing the energy economy to begin the switch from diminishing fossil fuel reserves.

However, the source of the hydrogen to be used in these vehicles is still undetermined. The lack of naturally occurring hydrogen reserves mandates that the fuel be produced using another source of energy. Since hydrogen is being used merely as an energy carrier in this case, the closest powertrain competitor would be the battery electric vehicle (BEV).

The fuel cell compares poorly to the BEV from an efficiency standpoint; most fuel cells get a maximum efficiency of 60% (hydrogen-to-electricity), compared to 85%-95% efficiency of battery packs (chemical-to-electricity)[22]. This also does not account for the energy used to compress (or liquefy) the hydrogen. Infrastructure challenges related to distribution also mar the fuel cell's future potential. However, automotive investment in fuel cells remains high, ostensibly driven by perceived technology and economic advantages: There is evidence that mass-manufacturing battery costs will eventually be material-supply driven[22], which will stymie further cost reduction attempts, while fuel cell costs will be driven mainly by the platinum loading factor, which engineering is rapidly reducing. Further, batteries are still plagued by durability issues[22]; the cost to put the battery through a full charge/discharge cycle is not yet low enough to compete with ICE-vehicles, while fuel cell durability research continues to make great strides forward[14].

Proton Exchange Membrane (PEM) fuel cells, which are most suited for vehicular applications, work by converting the input reactant's chemical energy directly to electrical energy. In a PEM fuel cell stack, this is done using hydrogen and air as the reactants and directing them into the many cells that make up a stack. Each cell separates the hydrogen's protons and electrons using the proton exchange membrane. The proton moves through the membrane, and the electron performs work in an external circuit. The electrons, protons, and oxygen and are exhausted as liquid water as shown in figure 4-1.

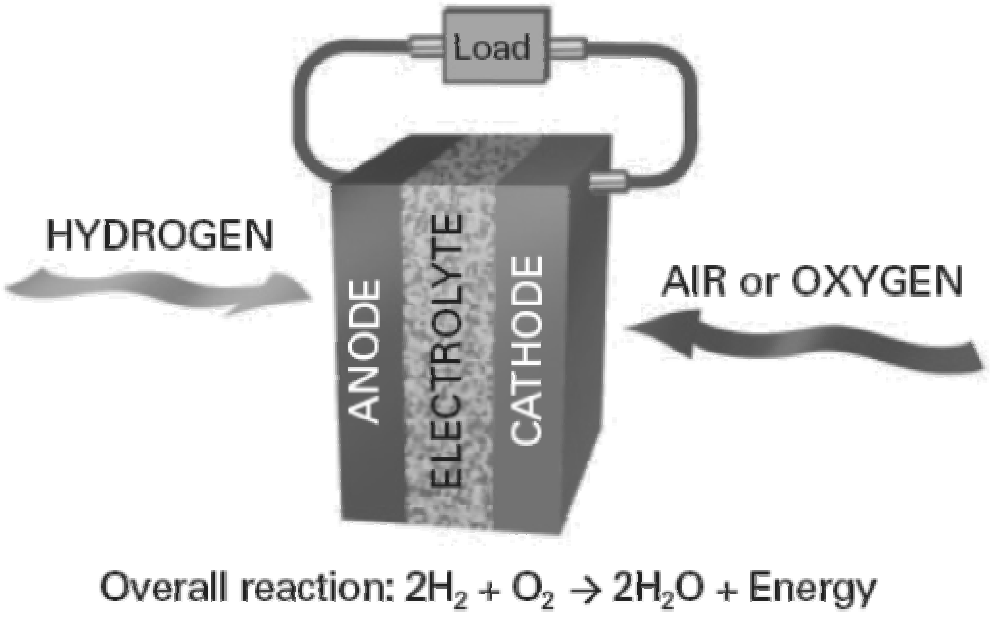

Figure 4-1: Fuel cell conceptual schematic[23]

There are number of technical problems that fuel cell vehicle designers are still grappling with, including:

- effective on-board hydrogen storage;
- the mass and volume of the fuel cell modules;
- durability and reliability of the cells; and
- cost.

4.1 Hydrogen Storage

There are four main methods to store hydrogen: hydrides, physisorption, high pressure storage, and liquid storage[24]. While most of these technologies have been developed to the point of being incorporated into experimental vehicles, the front runner is, unsurprisingly, pressurized storage. This is a well understood technology that has been used for many years in industrial and laboratory settings.

Unlike fuels that are liquid at room temperature, hydrogen has an extraordinarily low molecular density. Shrinking the hydrogen into a form that is useable can be energy intensive. The most commonly used form of hydrogen storage for automotive applications is compressed hydrogen. The stated goal[24] of compressed hydrogen manufacturers is to obtain 70 MPa cylinders, weighing only 110kg and storing 6.6 kg of hydrogen. This would yield a volumetric storage density of 30 kg/m^3 (compared to conventional gasoline, which has a storage density of 750 kg/m^3, neglecting tank weight)

4.2 Mass/Volume of Fuel Cells

The mass and volume of fuel cell modules is not yet comparable to ICE power plants. This is mainly due to the fuel cell plate design. Since the overall length of the stack is determined by the number of plates (cells), and the thickness of the plates comprising the majority of the overall thickness, optimizing the design of the plates is paramount in order to improve power density. This also means that their power is almost directly proportional to their size and mass, unlike an ICE, where the power (related to the displacement volume, which only comprises a small fraction of the whole engine volume), can scale up without a direct proportional increase in overall mass and volume.

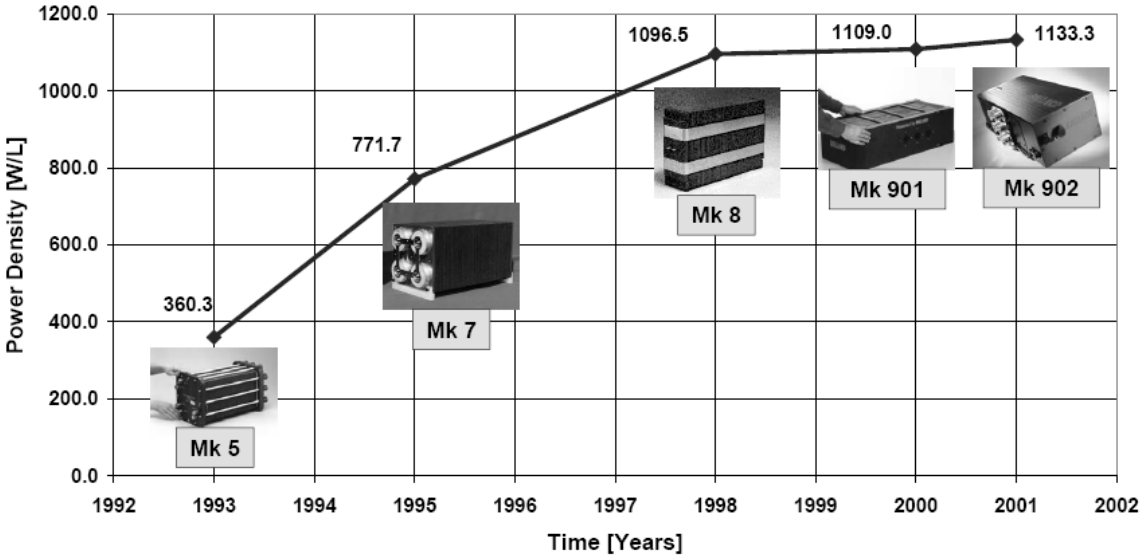

Figure 4-2: Ballard stack power density improvements over time

Fuel cell manufacturers have made enormous strides in reducing their stack volumes and mass as can be seen in figure 4-2[14], and they are getting very close to the power density equivalent to ICE, however they still have far to go due to the fundamental configuration of the vehicle:

- fuels cells produce only electric power, requiring an electric motor to convert the electrical energy to mechanical energy;
- while the stacks themselves are rapidly reducing in size, the parasitic components, such as hydrogen hydrators, air delivery systems, recirculation pumps, and control systems, still comprise a significant portion of the mass and volume. There is heavy research focused around designing these systems out of the fuel cell module[25];
- almost all fuel cell vehicles are still hybrid vehicles, requiring bulky energy storage systems and power electronics, along with their large size wiring and cooling systems; and
- hydrogen storage tanks are still very large due to the fundamental properties of the gas.

As a result of the above reasons, the majority of fuel cell vehicles utilize unconventional powertrain packaging, including, under the passenger compartment, or in the roof of the vehicle, and the rear cargo compartment. Figures 4-3 and 4-4 illustrate two examples of the approach manufacturers are taking to deal with the packaging issues caused by the volume of the components. The US DOE has set a target of 2000 W/kg as the viable limit at which fuel cell technology is capable of being incorporated into conventional vehicle platforms. Ballard Power believes it is capable of reaching that target by 2008[14], and will be able to reach 2500 W/L by 2010.

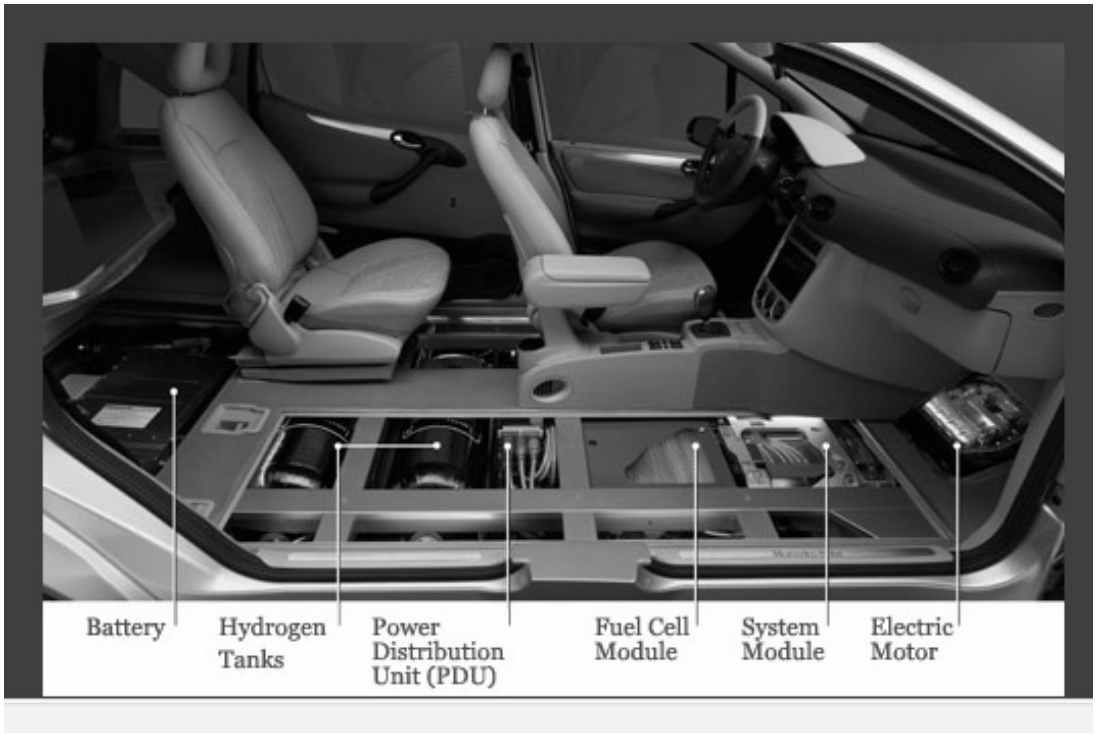

Figure 4-3: Mercedes 'F-Cell' vehicle component packaging cut-away[26]

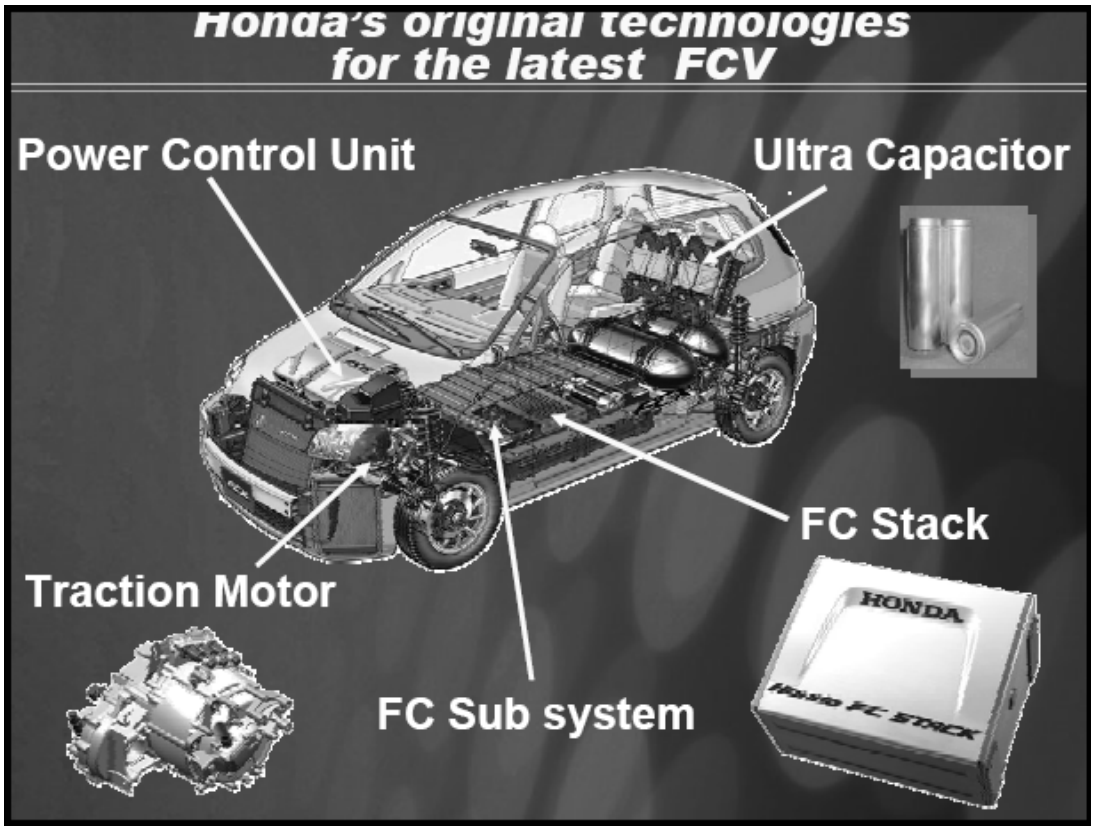

Figure 4-4: Honda Fuel cell vehicle component packaging[27].

4.3 Fuel Cell Durability

Fuel Cell stack reliability and durability, although widely believed to have the potential to be higher than ICE's due to the lack of moving parts, still has problems to overcome. The main issue surrounding fuel cell life involves membrane integrity, where pin holes develop in the proton exchange membrane, allowing hydrogen directly through to the oxygen-side, where it can react to form water via a combustion reaction. Other reliability issues involve the mechanical integrity and manufacturing quality of the stacks. Currently, manufacturing is a labor intensive process; most manufacturers are hand-building stacks, leading to issues with production quality. Figure 4-5[14] shows an example of a membrane pinhole.

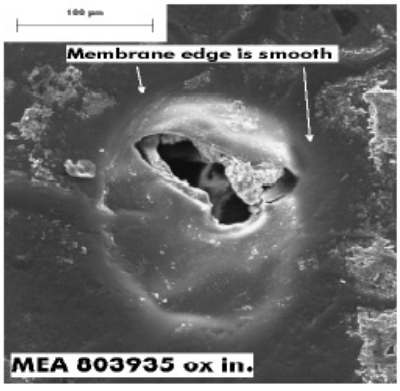

Figure 4-5: Membrane pinhole failure

4.4 Fuel Cell Costs

Currently fuel cells are still cost prohibitive for automotive applications: A ready-to-integrate fuel cell module would cost between 2000-20,000 $/kW at 2006 prices[23]. However, the majority of this cost is due to the prototype style manufacturing techniques still applied to each stack and the platinum content. The assembly of the stacks is still mainly done individually by technicians; increasing costs, and potentially decreasing quality.

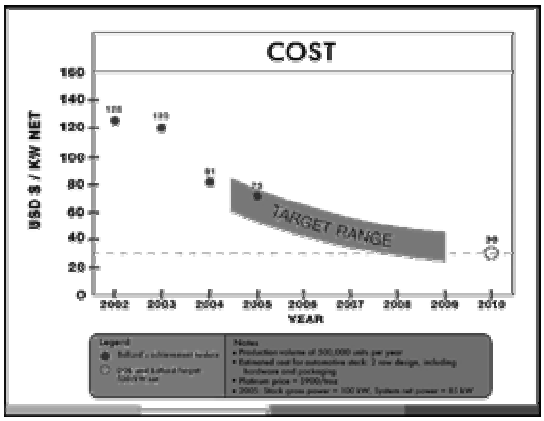

Figure 4-6: Ballard predicted future stack costs[14]

In a 2005 interview with Fuel Cell Works[28], Hydrogenics' CEO Pierre Rivard states that they had managed to cut costs 50% in the prior three years, and were currently manufacturing at 5,000-10,000 $/KW. Significant strides are being made in order to reduce the predicted cost of these stacks. Figure 4-6 shows Ballard's predicted costs of mass-manufactured stacks into 2010. They claim to have improved their technology enough that in 2005 they achieved a predicted mass-manufacturing cost of only $73/kW, and believe that by 2010 they can achieve 30 $/kW.

4.5 Current Fuel Cell Vehicles

Currently, there are a number of fuel cell vehicles in operation around the world, all of which are being used to generate real-world engineering data about powertrain operation. This world-wide fleet consists of small vehicles (Honda FCX, Daimler-Chrysler's F-Cell) and trucks, (GM's Sequel, Kia's Sportage)[29]. There are also a number of fuel cell bus fleets in Vancouver, Chicago, Perth, and in multiple locations in Europe. These vehicles are, in general, modified versions of production vehicles, with the exception being the series of fuel cell concept vehicles by GM (starting with the HyWire[25], and eventually updated to the Sequel[4]), which has radically changed conventional powertrain component packaging ideas.

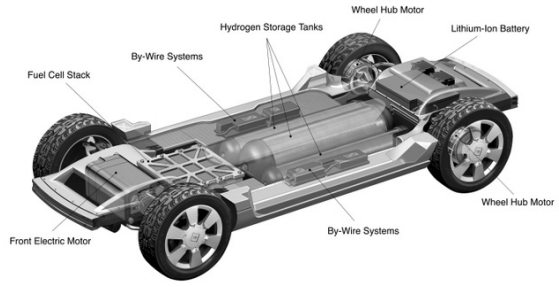

Figure 4-7: The HyWire powertrain packaging.

Figure 4-8: The production-ready Sequel powertrain packaging.

Most automotive manufacturers are looking to field fuel cell vehicles purely in an attempt to understand the powertrain characteristics. This is a normal process for powertrain development; generally new driveline components are retrofitted into existing vehicle platforms in order to validate their on-road performance before a platform is engineered specifically for them.

4.6 Fuel Cell Stack Sizing

There is an optimization that can be done in order to determine the optimum fuel cell size. Once the initial power sizing is done, which is determined by the power requirements of the consumer, it is possible to select the voltage (the number of cells), or the current (cell area) that optimizes efficiency within the limitations of: motor voltage constraints, DC/DC converter requirements, and battery voltage characteristics. Most fuel cell vehicles operate in the 200-400 VDC range.

4.7 Fuel Cell Vehicle Configurations

Currently most fuel cell vehicles are configured as hybrids; they include a high voltage battery pack and a high power DC/DC converters in order to boost overall power delivery, increase efficiency via load sharing, and enable regenerative braking. However, it has been expressed by multiple industry leaders that the ideal scenario is to see fuel cells increase in power (density) and efficiency to the point where the high voltage battery is not needed[25].

There are currently two topologies favored by the fuel cell vehicle designers: A battery hybridized fuel cell with a DC/DC voltage converter on the battery (Figure 4-9), and a non-hybridized fuel cell vehicle (Figure 4-10)[25]:

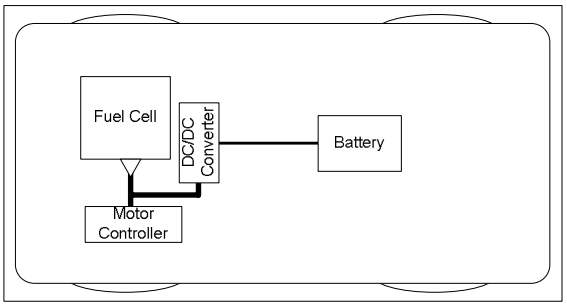

Figure 4-9: Hybridized fuel cell vehicle configuration

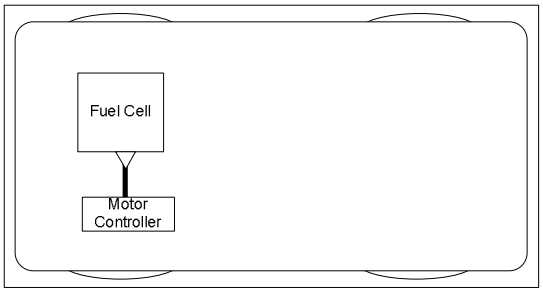

Figure 4-10: Non-hybridized fuel cell vehicle configuration

While the simpler configuration of Figure 4-10 is preferred in the long term, currently most manufacturers are opting to use a DC/DC converter regulated battery. This is generally more efficient than the other hybrid configuration, DC/DC converter regulating of the fuel cell stack, since the efficiency of the DC/DC (typically greater than 90%) is applied only to the energy entering and leaving the battery, which is, under most driving conditions, less than the amount of energy leaving the fuel cell stack.

4.8 UWAFT Fuel Cell Equinox

A hybrid fuel cell vehicle was created for the ChallengeX vehicle design competition. This vehicle was a four wheel drive with a total of 125 kW of electric power. The powertrain configuration can be seen in Figure 4-11 below:

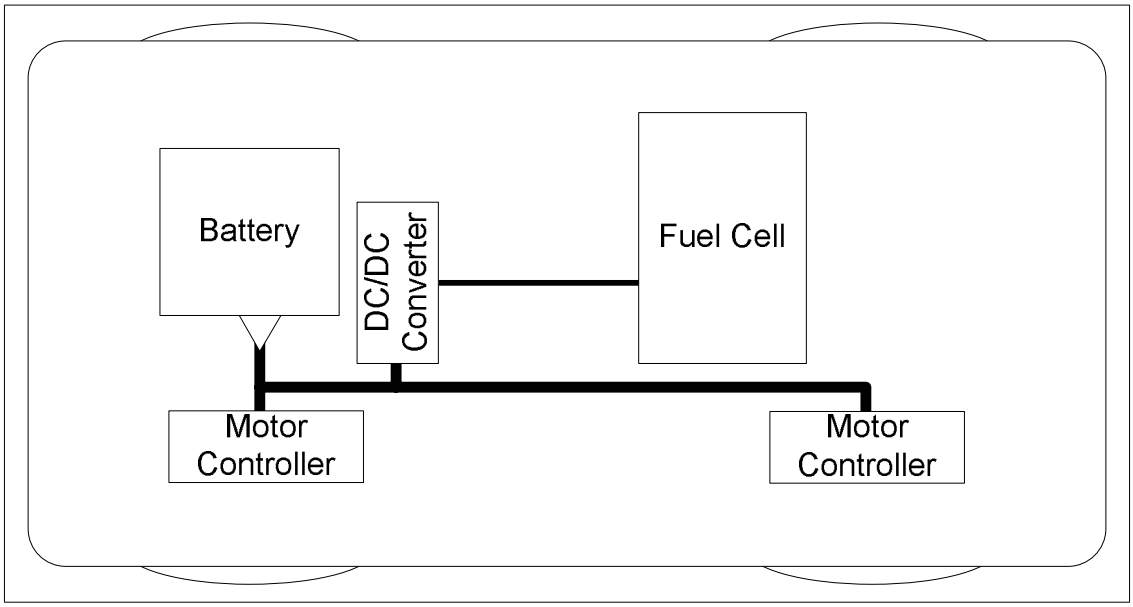

Figure 4-11: The UWAFT fuel cell Equinox powertrain configuration

Two integrated electric motor transaxles were implemented; one per axle that are capable of producing 67 kW of mechanical power each. Two motors we employed as a single suitably powerful electric motor was not available for purchase. The high voltage battery pack was rated for 60 kW (8.5 Ah) and had a nominal voltage of 288 V. The fuel cell was rated for 65 kW, and had an open circuit voltage of 310 V. Table 4-1 details more information on the specific powertrain components used in the design of the vehicle.

Table 4-1: Specification list for Fuel Cell Equinox vehicle

Device	Make/Model	Specifications	
Fuel Cell Stack	Hydrogenics/HYPM 65kW[30]	Max Power:	65kW
		Voltage Range:	190-300V
		Current Range:	0-300A
		Mass:	415kg
Hydrogen Storage	Dynetek/ZM180[31]	Max. Pressure:	5000psi
		Tank Capacity:	4.31kg
		Tank Weight:	92.kg
		Tank Volume:	178L
DC/DC Converter	Custom Waterloo Design[32]	Input Voltage Range:	190-300V
		Output Voltage Range:	300-385V
		Converter Type:	Boost
		Mass:	30kg
Motor Drive System	Ballard/312V67[33]	Peak Power:	67kW
		Continuous Power:	32kW
		Max Torque:	190Nm
		Mass:	84kg
Battery Pack	Cobasys/NiMHax 288-60[34]	Voltage Range:	322-392V
		Capacity:	8.5 Ah
		Energy:	2.8kwh
		Mass:	85kg

Table 4-2: Preliminary results of a virtual fuel cell Equinox[35]

Metric	Challenge X Targets	Waterloo VTS (65 kW)
Fuel Economy - combined EPA [L/100 km]	≤7.35	≤5.23
Mass [kg]	≤1996	≤2223
Acceleration: 0-100 km/h [s]	≤9.0	≤10.0
Acceleration: 80-110 km/h [s]	≤6.8	≤9.0
Range – highway [km]	≥320	≥240
Start Time [s]	≤5.0	≤5.0
Passenger Capacity	3,5	2,5
Emissions [Tier, bin]	Tier 2, Bin 5	Tier 2, Bin 1
Trailering Grade-ability 7% gr. – 90 km/h – 0.4 km [kg]	1135	1135 @ reduced speed
Trailering Grade-ability 4% gr. – 90 km/h – 9.7 km [kg]	1135	1135 @ reduced speed

4.8.1 Equinox Design and Design Methodology

The vehicle design began with the decision to pursue a fuel cell as the primary energy source. The initial sizing of the powertrain components was performed via a Design of Experiment analysis in order to determine the minimum size of components needed to fulfill the power (acceleration, trailering) and energy (range) metrics that the original Equinox vehicle had. A search for appropriate components was then undertaken in order to find the closest match to the results of the design of experiments. Once potentially viable components were selected, they were appraised in order to identify any negative interactions that could occur. This work was performed by the University of Waterloo's Alternative Fuels Team in 2004[7].

4.8.2 Component Selection using Design of Experiments

In order to identify optimally sized components that would allow the vehicle to achieve the performance required, a design of experiments approach was undertaken in order to map the design space in a reduced number of trials. The factors and levels were chosen as shown in Table 4-3[7].

Table 4-3: Categories and Factors used for the component selection D.O.E.

Category	Factors			
Vehicle Type	**Fuel Cell Power (kW)**	**Motor Power (kW)**	**Motor Efficiency (0,1)**	**Number of Energy Storage Cells**
Fuel Cell Ultra-Caps	25	60	0.95	120
	34.1	73.2	0.96	168
	47.5	92.5	0.97	240
	60.9	111.8	0.99	312
	70	125	1	360
Fuel Cell NiMH	10	60	0.95	200
	20	75	0.963	255
	30	90	0.975	310
	40	105	0.988	365
	50	120	1	420
Fuel Cell Li-Ion	10	60	0.95	240
	20	75	0.963	311
	30	90	0.975	383
	40	105	0.988	454
	50	120	1	525

This method helped the selection of an appropriate fuel cell, motor and energy storage sizing, along with generating information on the impact of selecting different energy storage

technologies, in particular: ultra-capacitors, nickel-metal hydride, and lithium-ion. Some of the results can be seen in Table 4-10[36] and Table 4-11[36].

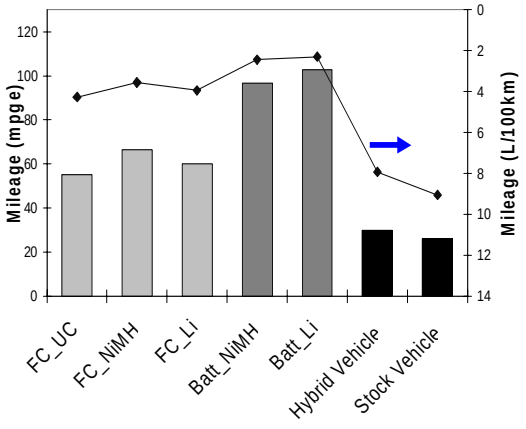

Figure 4-12: Mileage results component selection DOE

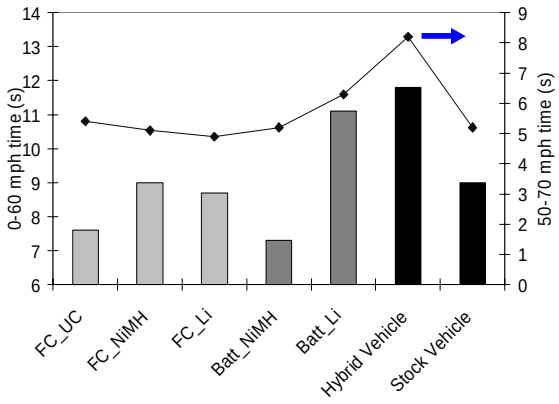

Figure 4-13: 0-60 mph acceleration results from component selection DOE

Figure 4-12 shows the impact of different configurations/energy storage chemistries on mileage (bar denote mpge, line denotes L/100km). Figure 4-13 shows the predicted acceleration of each vehicle. These results gave the alternative fuels team the direction to move the vehicle design towards. As a result of these statistical studies and the optimization of the design space that followed, the optimum powertrain was shown to be a fuel cell-NiMH (FC_NIMH), with the characteristics shown in Table 4-4.

Table 4-4: Optimum component selection driven by DOE results

	Parameter	FC_NIMH
Inputs	Engine/Fuel Cell Power (kW)	45.97
	Motor Power (kW)	86.56
	Peak Motor Efficiency	98.0%
	Number of ESS Cells	240
Outputs	IVM-60 mph (s)	9.0
	50-70 mph (s)	5.1
	Combined Energy Use (Wh)	8994
	Mileage (mpge)	66.3
	FC/ENG Efficiency	51.9%
	Motor Efficiency	88.0%
	Mass (kg)	1978.7

4.8.3 Selection of Appropriate Components

Once these 'optimized' components had been selected, a survey of commercially available components was done in order to assess the best fit and to detect lower level (communication interfaces, voltage matching, target application) compatibility issues. Components selected were as follows:

- a 65kw fuel cell;
- a 70kw battery pack;
- two 67kw motors; and
- a 4.31 kg hydrogen storage tank.

In addition, a 250-400 volt DC/DC boost converter was commissioned[7] in order to voltage-match the fuel cell to the high voltage battery. The components were connected in the manner shown in figure 4-11.

4.8.4 Voltage Compatibility Issues

Early in the design phase it became apparent that a compromise on the power from the battery was necessary due to the voltage limits from the motor system. In figure 4-14, the voltage-current relationships of the powertrain components are shown, including the valid motor operating regime (inside the trapezoid), the polarization curve of the 65kw fuel cell, and the voltage-current relationship of two batteries that were prime candidates. It is clear that the majority of charging current for the 336V battery is outside of the motor operating range, and that the 288V battery, for the same reason, cannot produce its maximum amount of current. The implication is that the combination of strict motor voltage limits and too high battery resistance restrict the ability of the powertrain to draw maximum power and to maximize regenerative braking. Data points in figure 4-14 were slightly modified from manufacturer-provided data to respect confidentiality agreements, however the modification bear no impact on the issues highlighted.

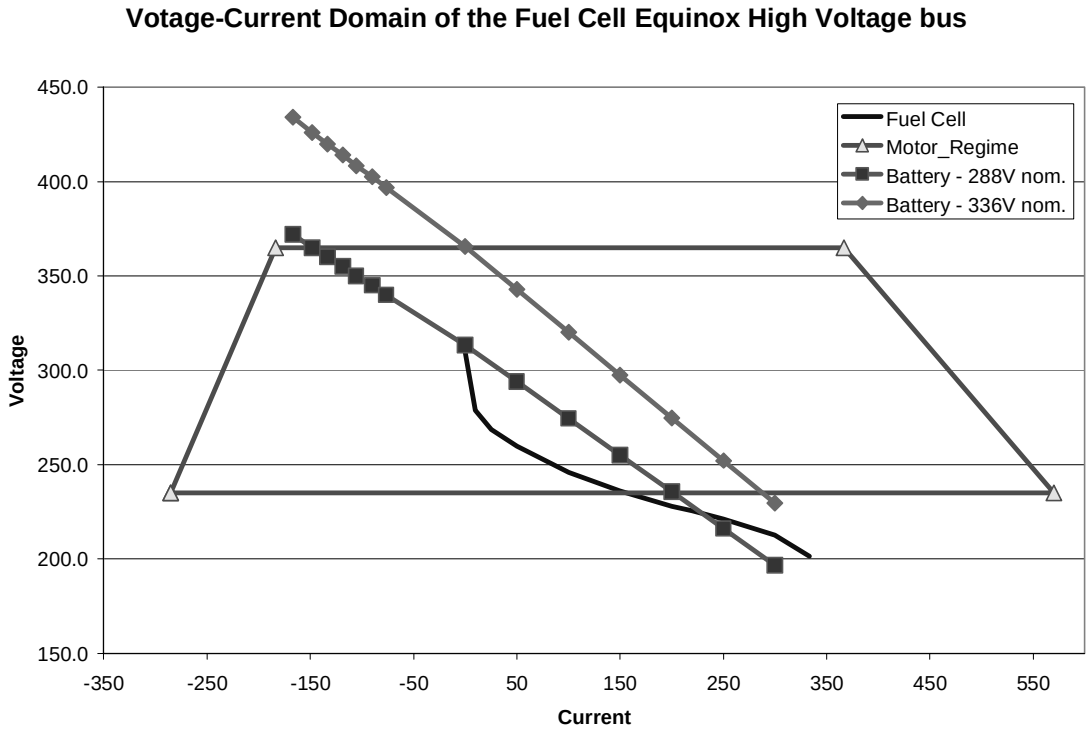

Figure 4-14: The voltage/current domain of the fuel cell vehicle

The upper voltage limit of the motors is in-fact two fold: There is a lower software limit (365VDC) that, upon detection by the motor inverter software, will automatically cease all motor operations. This limit is set to provide a small buffer to the second, IGBT-based limits of 380VDC (these IGBTs, in this design, are limited to 380VDC). These limits have to do with the maximum voltage limit inherent to any IGBT; the voltage spikes that occur when high frequency switching of an inductive load can cause catastrophic rupture of the IGBT module if the peak voltage is allowed to exceed the rating of the device.

In the end, it was decided that recouping braking energy, and improving fuel economy as a result, was more important than improving acceleration performance, and the lower voltage 288V pack was chosen.

It should be noted that even though the fuel cell voltage falls outside the motor voltage range at high power output, the presence of the DC/DC converter allows the voltage to be boosted to within those limits, thus the fuel cell can always deliver full power.

Another interesting consequence that developed as a result of the powertrain configuration was the voltage-dragging interaction between the battery and the fuel cell. Figure 4-15 illustrates the

high power DC/DC converter that was used in the vehicle (boosting section only – input and output filters not shown). This converter was designed and built by Jennifer Marshall, an electrical engineering PhD student during 2004-2005[32,7].

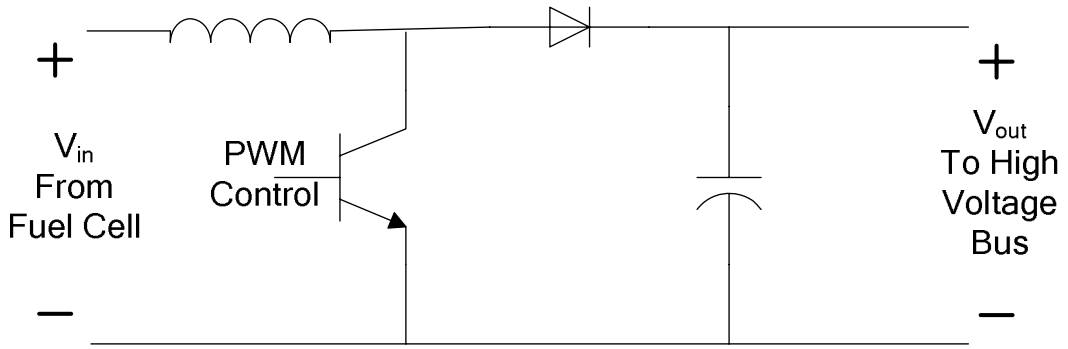

Figure 4-15: High power DC/DC converter boosting topology used in the Fuel Cell Equinox

This type of converter can boost the input voltage only. It is not bi-directional (current may only flow forwards due to the diode in order to protect the fuel cell), nor will it allow the output voltage to be controlled lower than the input voltage. Thus, if the output voltage is brought lower than the input voltage, current will flow uncontrolled through the diode and out to the load. This topology created two problems for vehicle development: dynamic high power testing, the runtime switching to a battery-only electric vehicle.

1. Testing became problematic without a dynamic electrical load. Testing of the DC/DC converter was done using a high power 300 V battery pack, into a resistor bank. However, due to the boost-only characteristic of the converter, as soon as the converter was attached to the load, large amounts of current would flow instantaneously, and continuously until it was switched out – there was no capacity to slow-ramp the current from zero (this would require a converter capable of bucking the output voltage). Once the load was switched on, the converter could control the current to higher levels, but could never reduce it beyond the initial value. In order to effectively test the converter (within the constraints of high startup current), a high voltage DC-rated contactor was used to switch the current on/off.
2. If a significant power demand is required from the vehicle, the battery voltage will begin to sag as it begins to deliver power. The boosting diode will become forward biased, and the fuel cell will be forced to start down its own polarization curve (start producing power), following the battery voltage (minus the minor volt drop across the diode, approximately 1.5 volts). This precludes the vehicle from running in pure electric mode seamlessly. The simple workaround is that the fuel cell must be connected/disconnected from the high voltage line before the vehicle transforms

from/to a battery electric vehicle. This is done by controlling the fuel cell current to zero temporarily (by disabling of the motors), and releasing the high voltage contactor that connects the fuel cell to the DC/DC converter. More information about these issues can be found in the UWAFT SAE technical documentation[7].

4.8.5 Updated Model Predictions

Once the implications of the relevant voltage issues were understood clearly, the vehicle models were updated, and the simulations were run again in order to generate new performance metrics. Table 4-5 shows the results of dynamic simulations, including the known system transients (fuel cell ramp time), and the controller code implemented into the vehicle.

Table 4-5: Updated vehicle performance metrics (compare to Table 4-2)

Acceleration Metric (kph)	Time to complete acceleration (s)
IVM*-100	12
80-110	9

*IVM = Initial Vehicle Movement

4.8.6 Hybrid Control System

Since all hybrid vehicles incorporate an energy storage system, and the ability to release that energy as appropriate, they need a strategy to manage this energy. One requirement of the energy management system is autonomy; no driver input is allowed, other than through conventional means (throttle and brake pedals).

Because of this requirement, the vehicle designers must include computer algorithms that decide when the vehicle enters certain modes, when and how it splits the power between energy sources, and when to shutdown certain systems. This algorithm is called the 'hybrid control strategy'. The algorithms must account for the following criteria:

- maximize fuel economy;
- maximize powertrain reliability/life;
- maximize redundancy in order to enable limp-home states;
- transient thermal constraints; and
- maximize drivability.

There are many different proposed methods available to achieve these goals. The Equinox fuel cell vehicle was built using a real-time optimization routine that incorporated only three different metrics:

1. maximization of overall powertrain efficiency;
2. reduce fuel cell shutdown/startups in order to improve reliability; and
3. state-of-Charge (SOC) targeting to improve battery life and improve acceleration performance.

The algorithm works to find the ratio of power to be delivered from the fuel cell and the battery, and acts to deliver that power via closed loop control over the current flowing from the fuel cell through the DC/DC converter. The algorithm is executed every 10 msec and is as follows:

1. Determine how much power the motors will require in the next 10 msec based upon the torque request, the motor speed, and the motor efficiency maps
2. Determine the maximum and minimum power that can possibly be delivered from the battery pack:
    a. The maximum is determined by the allowable current from the battery (as determined by it's internal processor)
    b. The minimum is determined by the amount the battery can absorb (as determined by its internal processor), and by the amount of power the fuel cell can produce.
3. Estimate the overall efficiency of the powertrain at each of 10 different battery currents, between the maximum and minimum,
4. Weigh the result with the other factors (fuel cell shutdown counter, Battery State of Charge) and choose the optimum solution.

This algorithm is adapted from research performed at the National Renewable Energy Laboratory[6].

Chapter 5

AC Induction Tractive Motor Technology

This section will focus on the specifics of AC induction motors. Both the Fuel Cell Equinox and the HEV Pacifica use AC induction technology to power the vehicle. Other motor technologies will not be covered here; however the technical concepts between motor types are similar, and require little modification to apply to Permanent Magnet or Switched Reluctance motors.

5.1 Motor Control

Induction motors rely on a set of three windings encased in the non-rotating case to induct current into the (rotating) rotor of the machine, which in turn produces the needed rotor magnetic field. Unlike permanent magnet motors, which rely on rare earth magnets to provide rotor magnetization, this method requires the stator currents to provide the energy to magnetize the rotor. There are numerous benefits to this approach, making induction machines the technological leader in industrial applications, specifically;

- Induction machines generally have more robust rotors, due to the simplicity of their design (no additional structural support is needed to restrain the magnets or coils against centrifugal forces), allowing faster possible speeds and reduced rotational inertia, along with improved reliability;
- Induction machines have no brushes to wear, to spark, or to produce dust, unlike DC motors or Universal-type motors. They are brushless, and can be run directly from any AC source, including synthesized AC voltages (ie. from a power inverter);
- While in the industrial setting, it is common to find AC induction motors run directly from the AC voltages present ‘at the wall’, it is also possible to synthesize alternating current using solid state switches. This allows the generation of variable frequency, variable voltage power, enabling the introduction of ‘vector controlled’ drives;
- Induction machines are generally cheaper than permanent magnets or DC machines as they have only a single set of windings, and no expensive magnets. They are generally of simpler construction than other types of motors; and
- AC induction motors also have very low no-load resistance torque, due to the lack of any significant magnetic flux contained within the rotor.

Vector control is an algorithmic approach to transforming the requested torque (and magnetic flux) to the three phase currents that the six power switches control (see figure 5-1). The core of this algorithm implements closed loop control over the three phase current, and uses two geometric transformations (the “Clarke transformation” and the “Park transformation”) to change the torque and flux into the three-phase current.

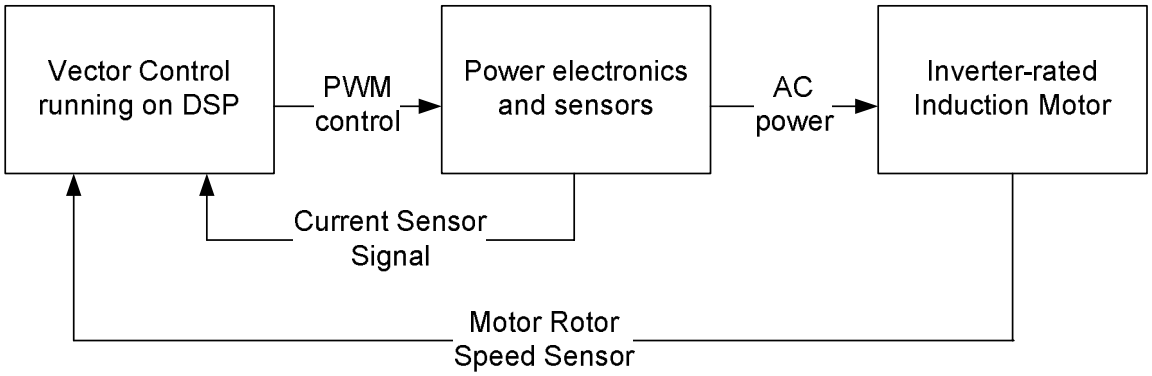

Figure 5-1: The high level component schematic of the motor drive system.

5.1.1 Clarke Transformation

Since the currents of any balanced three-phase system sum to 0, there are only ever two degrees of freedom within the system – the current amplitude in any two phases. These three phases can be transformed into a 2-axis 'direct and quadrature' system using the Clarke Transformation[37]. This 2-axis system is static relative to the stator (the motor housing), and can be transformed as follows:

$$i_{ds} = i_u$$

$$i_{qs} = \frac{1}{\sqrt{3}}(i_u) + \frac{2}{\sqrt{3}}(i_v)$$

Where:

- i_u, i_v, i_w are the three phases of the stator current (i_w has been eliminated from the above equations since $i_u + i_v + i_w = 0$)
- i_{qs}, i_{ds} are the quadrature and the direct current components in the stator frame

5.1.2 Park Transformation

Once the Clarke transformation has been completed, the 'dq – stator' coordinate system can be transformed into the rotating rotor system, the 'dq – rotor' frame, using the 'Park Transformation'[37]:

$$i_{ds}^{r} = i_{qs} \sin\theta_r + i_{ds} \cos\theta_r$$

$$i_{qs}^{r} = i_{qs} \cos\theta_r - i_{ds} \sin\theta_r$$

Where:

- i_{qs}, i_{ds} are the quadrature and the direct current components in the stator frame

- i^r_{qs}, i^r_{ds} are the quadrature and the direct current components in the rotor frame. These are significant since they can be viewed as the currents that provide the torque and the magnetic flux to the rotor, respectively, and thus they can be placed under closed loop control to control the operation of the motor.
- θ_r is the angular position of the flux (since the flux is slipping relative to the stator currents, this value is not simply the angular position of the rotor, but the sum of the rotor angle and the slip angle)

5.1.3 Vector Control

The Park and the Clarke transformations are used in the vector control method to produce an estimate of the torque: $T \alpha i^r_{ds} i^r_{qs}$. This algorithm can be seen in block format in figure 5-2:

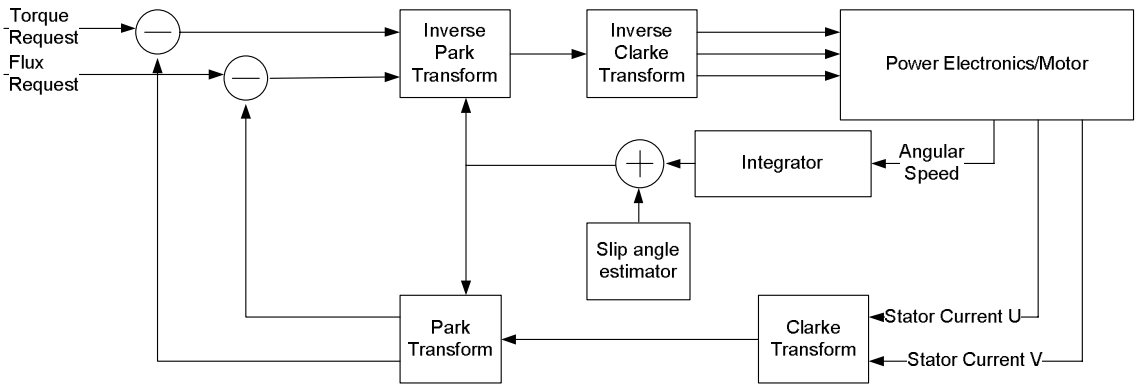

Figure 5-2: Vector Control Algorithm for an AC induction motor

The net result of using this type of control is the independent control of torque[37]. Unlike AC line-driven motors, where the speed is purely determined by the load conditions, the vector controlled motor can control the load speed via its torque control. This is necessary for a vehicle application.

5.2 Motor Drive Losses

There are a variety of losses that occur inside the motor drive system. They are dependant on a wide variety of parameters. Some of these are listed below:

1. PWM harmonics – The sine waves created by the inverter are digital, they are not true sine waves, and the associated harmonics creates losses within the motor. This loss is dependant on the ability of the inverter to create clean sine waves, and thus depends highly on the speed of the motor and of the switching frequency.

2. Rotor Magnetization – Some amount of current is needed to magnetize the rotor in an induction machine. This current is not acting to directly create torque, and so is a parasitic loss on the system. Generally, the rotor current is greatest in the constant torque region, and reduces as speed increases.
3. Switch conduction losses – The switches generally exhibit some small ‘on resistance’ while conducting current. This loss heats the switch and must be removed by a cooling mechanism. This loss is proportional to the duty cycle of the PWM signal.
4. Switching losses – The switches, upon turning off, rapidly increase their resistance while simultaneously decreasing their current throughput. There is a brief period where the resistance and the current are high, and some energy is lost. A similar phenomenon occurs upon ‘turn on’. This loss is proportional to the switching frequency of the inverter.
5. Motor Losses – The motor has internal resistances which reduce efficiency. There are also losses occurring due to inducted eddy currents in the motor case. These losses are generally dependant on the current flow.
6. Mechanical Losses – There are a set of mechanical losses that occur through the gearbox and the differential, to the constant-velocity (CV) and tripod joints. These are generally a function of the speed of the motor.

Chapter 6

Torque Control: Problem Definition, Solution and Simulation

Modern research and development into vehicles powered by electric motors started with GM's Impact electric vehicle in 1990. The successful deployment of this vehicle (eventually called the EV-1[38]) to the marketplace spurred the California Air Resources Board (CARB)[39] to introduce the zero emission vehicle (ZEV) mandate, specifying that all manufacturers who wished to sell vehicles in California, must have ZEV's comprise 2% of all sales by 2003. However, in April 2003, CARB approved the "Alternative Compliance", allowing the relaxation of the EV mandate in order to allow automotive manufacturers to pursue fuel cell vehicles[40].

All vehicles produced in response to the EV mandate were relatively low powered front wheel drive models. This fact presumably arose for three reasons:

1. the vehicle power was limited by the batteries;
2. the manufacturers were still grappling with vehicle range issues (again, due to their battery technology); using smaller motors helped in this regard by reducing overall mass, and limiting power draw; and
3. front wheel drive vehicles were easier to integrate, since many of these vehicles were simply variants of existing ICE powered vehicles, and also upheld the favorable vehicle handling and stability characteristics that their host vehicles had been designed for.

However, as electric vehicles start to move further into what is traditionally internal combustion engine territory, eventually all wheel drive vehicles will start to be converted as well. Those systems may take the form of a single motor driving a transfer case, much like conventional 4-wheel drive vehicles, or it may mean two, or even four separate motors, each driving an axle, or wheel respectively. This additional torque control over each wheel or axle allows the vehicle designer much more control over the dynamic behavior of the vehicle, and the chance to improve the stability of the vehicle using advanced traction management strategies. However, since one of the stated goals of these advanced vehicles is to improve overall efficiency, it is also of interest to know the impact of a specific torque splitting algorithm upon the power train efficiency: is there an optimum way to share torque between motors? And what is the potential for efficiency gain?

Since both the Equinox and the Pacifica have two AC induction motors, the question about how torque will be controlled must be addressed. In order to solve the problem in its entirety, the following issues must be addressed:

- Efficiency – is there an optimum algorithm which will improve the overall efficiency?

- Traction – How should the control strategy deal with limited friction situations?
- Stability – How does the torque control algorithm avoid negatively changing the oversteer/understeer characteristics of the vehicle? How is driver startle avoided?
- Braking – how can regenerative braking be maximized? How can tire slip during braking be avoided? What is the transient behavior of the motors during tire lockup?
- Drivability – how does the torque splitting algorithm affect a qualitative evaluation of the vehicles power-train performance?

The primary objective of this work was to develop a torque splitting algorithm that can minimize energy consumption while producing the torque the driver requests *in a transparent manner*. This thesis does *not* evaluate the impact of demand-shaping driver intent. No attempt is made to modify or mitigate the torque and speed desires of the driver. It may be possible to achieve this influence over the driver by tuning vehicle responsiveness, but for the purposes of this work, depression of the throttle pedal will proportionally generate vehicle acceleration. Further, one key assumption for this work is that driver speed and acceleration demands will be an input to the algorithms; it cannot be influenced.

However, this objective of transparency cannot be realized without considering the dynamic stability, drive quality, and traction control implications.

The solution to this problem will be presented in a number of steps:

1. the initial assessment of the problem, including addressing the feasibility of a solution;
2. the development of an algorithmic framework that will be used in the vehicle. This will create a structure into which a solution may be inserted;
3. a set of vehicle simulators that will be used to test control algorithms; and
4. a proposed solution and the simulation results

6.1 Solution feasibility

It was proposed that by sharing torque between two motors at a given motor speed, the overall efficiency of the powertrain can be improved. By examining the efficiency plots of the motors, two opportunities were identified:

1. reducing time spent at very low torque values can cut losses;
2. below 4000 rpm, there are torque values which may be targeted to reduce losses

These opportunities will be examined in detail in sections 6.2.1 and 6.2.2.

6.1.1 Low torque levels

Figure 6-1 shows the motor system efficiency (high voltage DC electrical power in to mechanical power out) at a motor speed of 2500 rpm[41]. While the motor demonstrates a mostly high, flat curve, the efficiency at zero torque drops to zero as expected. This seems to indicate that operating the motor at torque levels less than 10 Nm implies large losses. However, there are a few assumptions that must be addressed in order to understand the issues at play, before such a statement can be made.

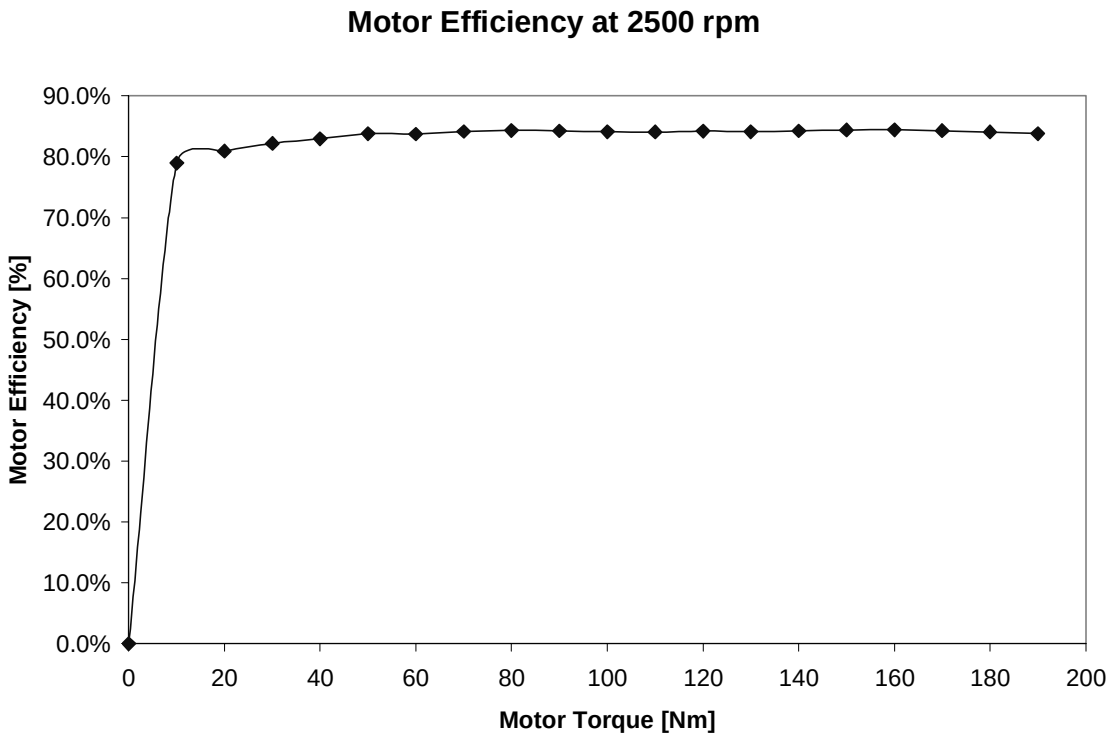

Figure 6-1: Motor system (inverter + motor) efficiency curve (Mechanical Power/ Inverter Power) at 2500 rpm rotor speed.

The efficiency data used in this work was generated by Ballard Power Systems[42] as part of their internal motor testing. They measured bus voltage and current and compare that to the measured motor speed and torque. This yielded the total efficiency across the spectrum for the motors, which is used throughout this thesis. Lacking data between 0 Nm and 10 Nm, it was assumed that the efficiency curve was linear through this section – further testing should be performed in this

region to identify the true value. The total impact of this region is small; while the efficiency is low below 10 Nm, the total power output is also small, thus creating small impact on the results.

There is a 150 watt constant load applied by the inverter: this load is accounted if the efficiency is non-zero, however at zero output power (no speed or torque), this additional load must be added.

6.1.2 Efficiency Targeting

Figure 6-2 shows the efficiency of the motor system over the operational limits of the motor. The grayscale legend indicates the efficiency, with the majority of the motor region exhibiting high efficiency (greater than 80%). The motors have low efficiency at very low speeds or torques. The grayscale does not have enough resolution to identify the maximum efficiency with respect to speed; thus the solid line indicates this maximum. Note that the line corresponds to the maximum possible motor torque at and above 4000 rpm, but the line's behavior is non-intuitive below this speed.

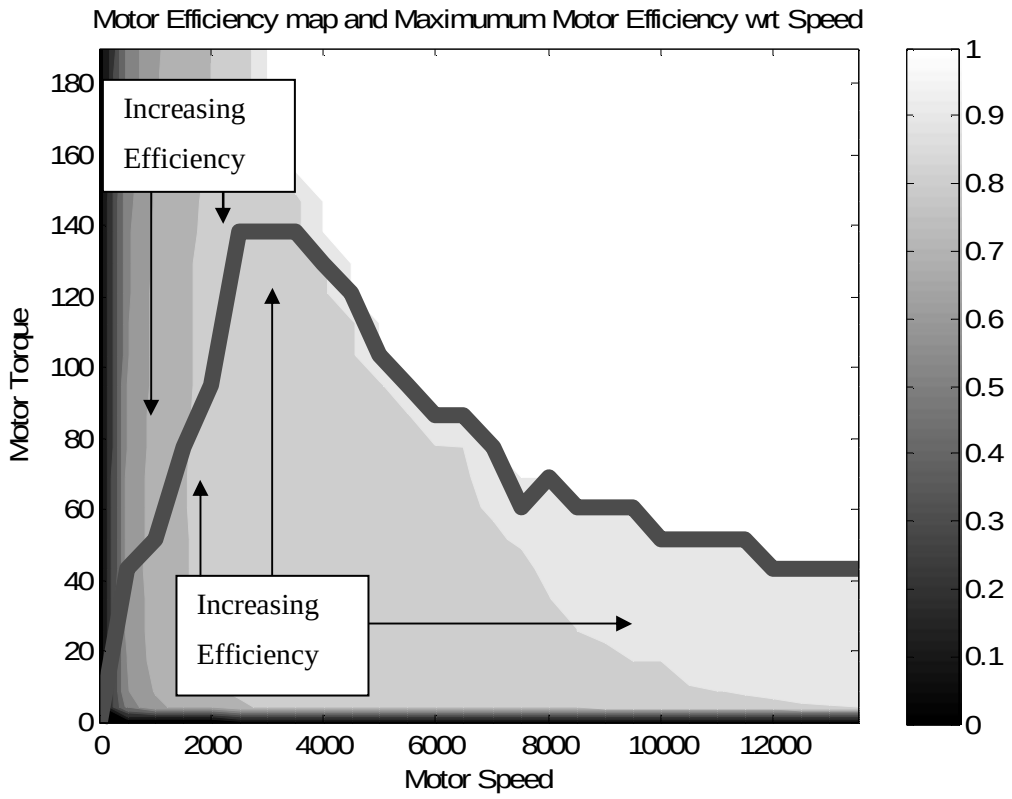

Figure 6-2: Motor efficiency map. The solid line indicates the maximum efficiency relative to motor speed.

In order to improve efficiency, a strategy must involve targeting the solid line. The following strategy is proposed:

- If the requested torque is higher than the peak efficiency torque (thus operating the motor above the solid line in figure 6-2), then torque is split between motors in order to drive the motors down to a more efficient operating point.
- If the requested torque is equal or less than the peak efficiency torque, then all the torque is delivered by a single motor to increase overall efficiency (to get as close as possible to the solid line).

While this work attempts to derive an optimum method to control torque distribution in existing vehicles, there is also the potential to use these same efficiency considerations during the design process of selecting motors. For example, upsizing or downsizing the motor may allow the vehicle to better target the maximum efficiency line. This idea will not be examined in this thesis, but can be readily addressed by systematically tuning the simulation code presented herein to evaluate different sizes of motors in different sized vehicles.

6.2 Control Details

The hardware and software needed to accurately and safely control the motors is complex and multilayered. In order to provide context for the problem, a brief overview of the hardware and software layers will be given. Then, an explanation of the error detection systems that make the vehicle torque control system failsafe is presented. The specific problem that needs to be solved will then be addressed.

6.2.1 Hardware/Software layers

The original equipment communications network on the Equinox consists of two separate systems. The high speed system, complying with the automotive specification called CANbus[43], links the powertrain components together. The engine controller (ECM), the transmission controller (TCM), and the electronic braking system (ECBM) use this network to communicate. This can be seen in figure 6-3. In addition, the body controller acts as a gateway to transit data from the CANbus to the low speed Class2 network and vice versa. The Class2 network acts to support non-powertrain systems, such as the radio, the instrument panel, the power steering system, and the airbag system. GM also included an OnSTAR[44] system in this vehicle, whose controller can communicate on both the CANbus and the Class2 network.

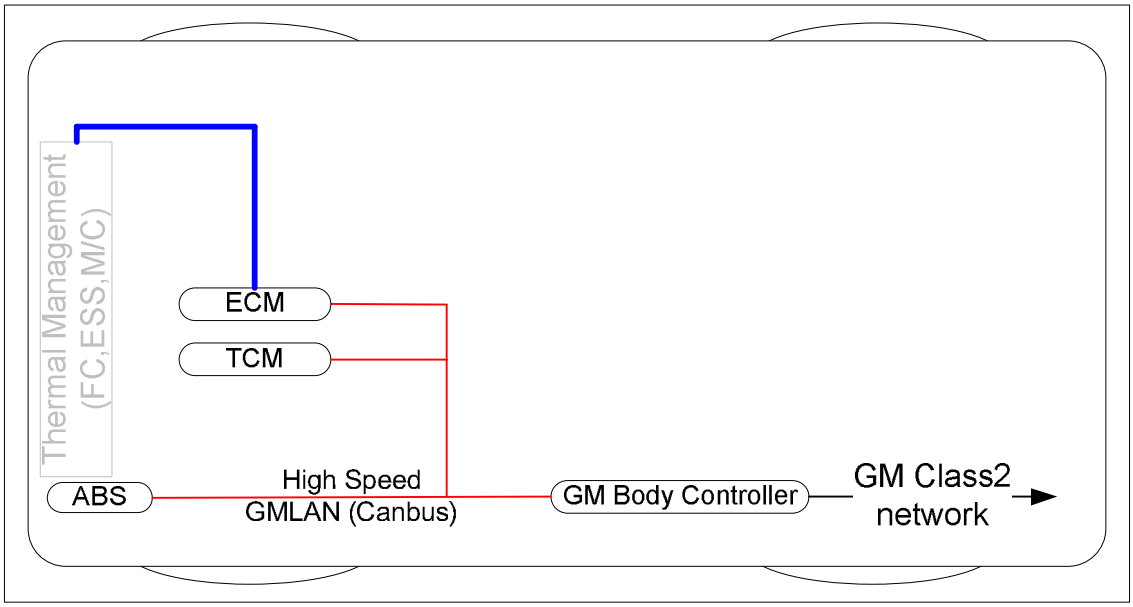

Figure 6-3: The original CANbus system implemented on the GM Equinox. Showing only OEM powertrain related devices.

The modifications made to the in-vehicle system consisted only of removing the ECM and the TCM. The removal of these modules would normally cause multiple faults propagating from the ECBM and the body control throughout the vehicles computer network. However, the signals normally generated by the ECM and TCM were recreated by the implementation of custom vehicle controller units (VCU's). The GM Class2 network was left wholly intact.

The CANbus is an industrial communications protocol that implements a variable bit-rate peer-to-peer network. The system is fault-tolerant and nodes can self-detect problems and turn off their transceivers in order to protect the integrity of the bus. Speeds can range up to 1 Mb/s throughput. The speed chosen for the Equinox implementation was 500Kb/s. Data is packed into messages of 8 byte length, which are assigned ID numbers. The lowest ID numbers have the highest transmission priority, and simultaneous transmission conflicts are arbitrated via the use of dominant/recessive bits according to the ID priority. The CANbus topology for the Equinox was designed primarily by Matt Stevens, a chemical engineering student, in order to manage each buses bandwidth, and to separate devices which have identical ID numbers.

There are five main powertrain devices in the fuel cell powered Equinox: two motors, a battery, a DC/DC converter, and a fuel cell. Of these five, four of them, all except the DC/DC converter, came preprogrammed with their own internal controllers supporting CANbus. These four devices could be communicated with and controlled by the vehicle control units (VCU's) using additional physical CANbus channels. There are two VCU's on-board this vehicle. Both devices were provided by an engine control company called 'Mototron'[45]. These units formed the hub of the communication system, receiving and interpreting the status and diagnostic information sent by each of the devices, and providing responses as needed. Figure 6-4 illustrates the different control modules in the fuel cell Equinox. The BCM (Battery control module), MCU (Motor control unit),

FCCM (Fuel Cell control module), VCU (vehicle control unit), EBCM (Electronic braking control module) and GM body controller (electronic body systems) are shown.

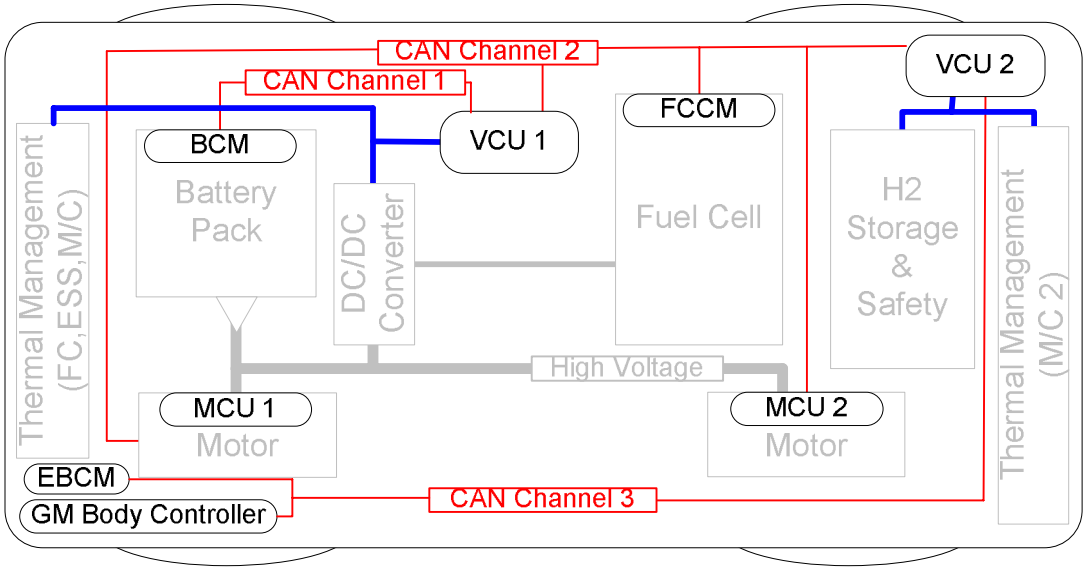

Figure 6-4: Vehicle layout of powertrain controllers.

The reason for two distinct VCU's in the vehicle was to get access to enough analog and digital input/output channels to control the various supporting subsystems such as pump and fan control, low voltage bus monitoring and control, air conditioning control, and powertrain component control. Each VCU has two CAN channels that may be accessed independently of each other. The two MCU's, being identical, originally had identical message ID's for all of their six control and diagnostic messages, this was changed at the factory in order to allow both controllers to reside on the same bus. Figure 6-5 shows the partitioning of VCU responsibilities, as well as the distribution of controllers on each CANbus. Also shown are some of the relevant inputs and outputs from each controller. As can be seen, VCU1 performs all powertrain control functions, while VCU2 acts to satisfy the EBCM and the body controller. Analog and digital I/O are not shown. More detail about each component and the control required will be presented in the next section. All code discussed in this thesis pertain only to VCU1.

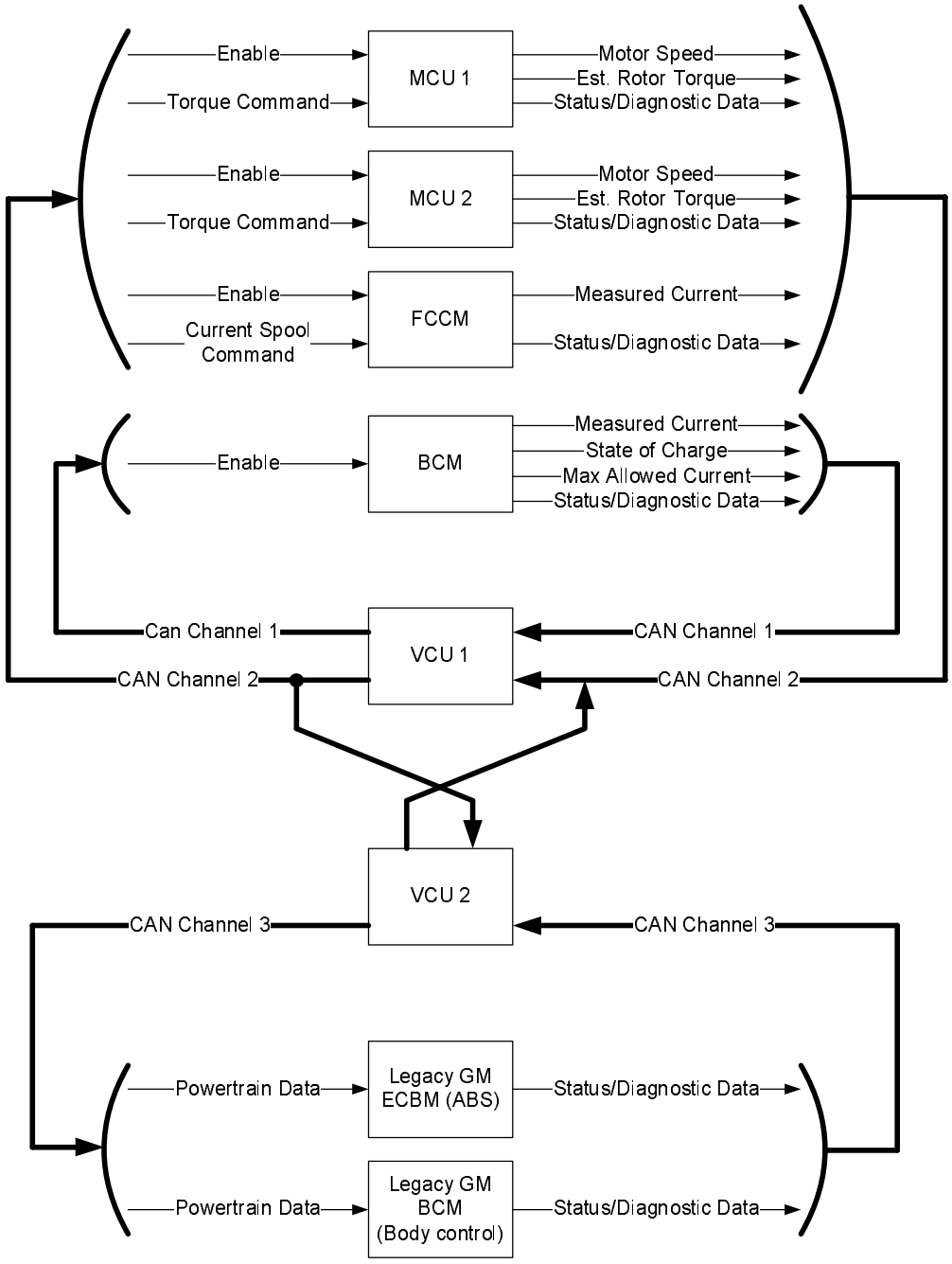

Figure 6-5: The partitioning of responsibilities between the two VCU's. VCU's communicate with each other using CAN channel 2. CAN channel 3 allows access to body electronics

6.2.2 Information available on the CANbus

There are a number of diagnostics and runtime information available through the CANbus networks and via analog input. For this algorithm development, only the following inputs and outputs identified in table 6-1 were used.

Table 6-1: The inputs and outputs used in the development of the Torque Control Strategy

Inputs	***Outputs***
Throttle position sensor	Torque request (front)
Motor Speed (front)	Torque request (rear)
Estimated motor torque (front)	
Motor Speed (rear)	
Estimated motor torque (rear)	
Measured battery current	
Allowed battery current	

6.2.3 Mototron Controllers

The VCU's that implemented vehicle-level functionality were provided by Mototron. These devices used standard Freescale[46] MPC555 and MPC565 automotive control processors. The interesting and unique aspect of these VCU's is the method of programming. All code is written in the Mathworks Simulink graphical language[47], making code easier to develop, compile and debug. This Simulink code is auto-code generated into C-code using the Mathworks Real-Time-Workshop, and then compiled for the MPC565/555 processor target using a compiler provided by Greenhills[48]. After compilation of the application, the code is downloaded via the CANbus to the controller's application memory and run. This is a complicated tool-chain and requires many steps and levels of software to accomplish. However, it allows the application to be created with very little knowledge of the embedded hardware.

Figure 6-6. shows the vehicle control code schematic that is used as a roadmap to implement the vehicle controller. There are three groups of code on the top level: processing of input signals, algorithms to generate vehicle control, and output processing. Within the vehicle control algorithms, there are many states. Four are shown: startup, fault, run, and shutdown. The only state of relevance here is the run state, active when the vehicle is in normal operating. Within this

run state, there are three pertinent questions: What is the best way to control the fuel cell, the DC/DC converter, and the motors? The code that this thesis deals with is solely in the torque control block at this level.

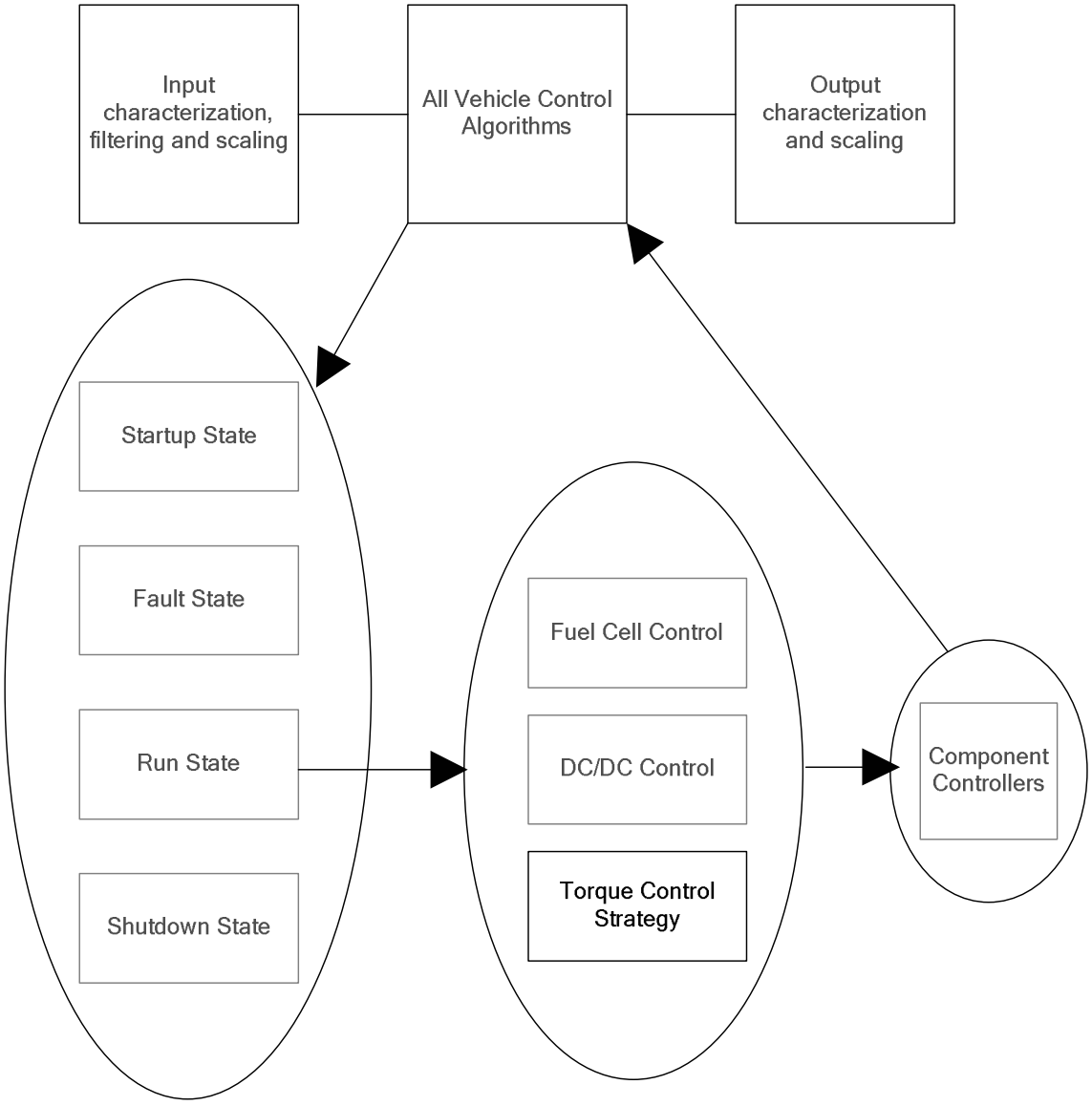

Figure 6-6: Schematic of Equinox control code. The Torque control strategy discussed in this thesis comprises an integral part in the vehicle's entire control scheme

Once the torque control strategy has been computed, the signal is passed to the component controllers, which verify that no safety triggers have been activated, and that the torque is safe to be released. The signal is then sent to the output block for scaling. It is run through a numeric

conversion in accordance with the specific CANbus message and passed to the Mototron CANbus implementation code for transmission to the physical CANbus.

6.2.4 Control Problem Scope and Description

Assuming that the problems of input/output and safety are solved adequately, and that the balance of the powertrain control is addressed (fuel cell control and DC/DC control), the torque control problem can be simplified to the following: Given the throttle pedal signal (TPS) value and certain powertrain operating conditions, what is the 'optimum' method to generate the front and the rear torque commands? The definition of 'optimum' encompasses Vehicle Stability, Traction, Efficiency and Powertrain protection.

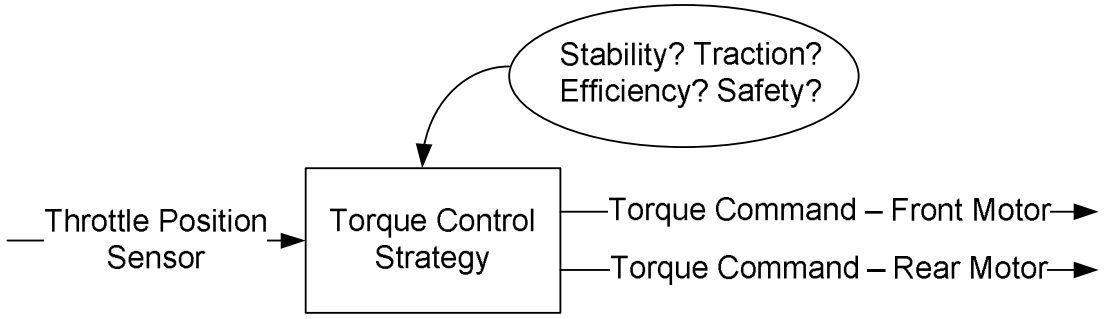

Figure 6-7: Problem Statement: Generate an algorithm to split torque between motors considering vehicle stability, traction and efficiency and powertrain protection.

In addition to the vehicle performance considerations (stability, traction, efficiency), the torque command directly imposes load on the power delivery system of the vehicle. Thus, this command must be generated in such a way to ensure that the fuel cell and battery remain within their operational regimes (maximum power draw and state of charge limits must be respected) and further, that while doing so, the TCS does not unduly constrain vehicle performance.

6.3 In-vehicle Controls Algorithmic structure

The design process began by devising a TCS structure, which was comprised of four functional subcomponents. Each of these sub-blocks would perform one important function of the algorithm. These four blocks are:

1. torque generation calculation (how much vehicular torque does the driver want, and how much can de delivered within the constraints of the powertrain?);

2. torque splitting calculation (how is the torque split between the motors?);
3. traction control (is there undue wheel slip? What corrective action should be taken?);
4. torque Arbitration (how to negotiate between the requests from the traction control algorithm and those of the torque splitting algorithm?).

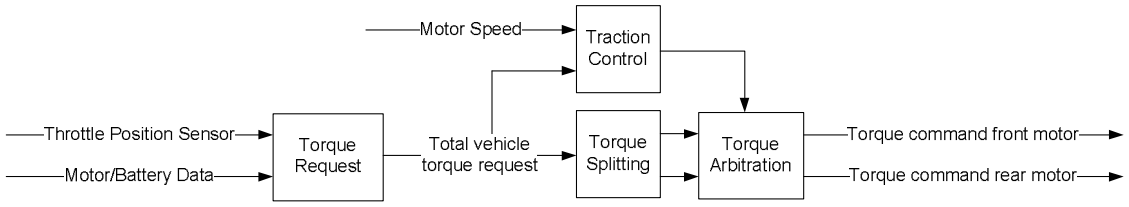

Figure 6-8: The torque control strategy algorithmic structure

6.4 Torque Control Algorithm

This section will give details of the code that runs on each of the four sub-blocks of the TCS. Torque generation, traction control and torque arbitration will be discussed in sufficient detail to allow the presentation of the torque splitting algorithm in section 6.6.

6.4.1 Torque Request

Producing a vehicle-wide torque request (VTR) involves fulfilling a number of issues:

- interpret driver intent;
- provide good drivability (fast response, controllable torque delivery, low jerk);
- ensure that the power drawn from the electric drivetrain is within the allowable battery and fuel cell limits at all times;
- provide the maximum possible power to the driver; and
- provide the smallest possible slew limits in order to decrease ‘spooling’ of acceleration (maximum torque is available to the driver as quickly as possible).

The chosen solution to fulfill these criteria is shown in figure 6-9. This is a two stage control system. Nominally, the maximum possible motor torque is simply scaled according to the throttle signal. However, upon small current errors (less than 5 Amps), the battery current controller will become active. When this occurs, the controller generates negative values, which act to reduce the

total torque command. This allows the full torque of the motor to be delivered up to the point where the battery becomes the limiting factor. This system allows the full delivery of available electrical power regardless of the state of the battery or the fuel cell. If the fuel cell is off, the motors will take up to the maximum possible from the battery. If the battery SOC is low and the battery current limit is low, then the motors will take up to what is available. The exact implementation of this code can be found in Appendix A.

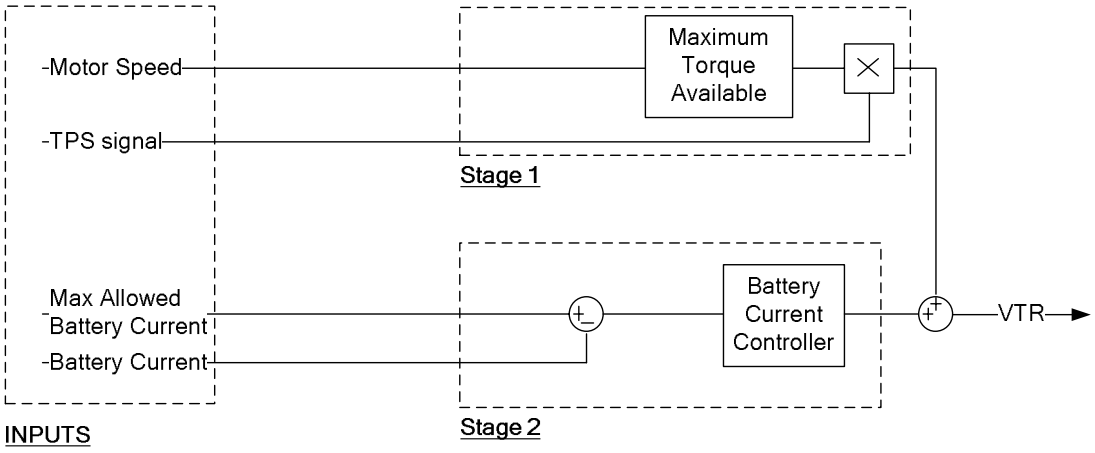

Figure 6-9: VTR generation algorithm

Both the instantaneous battery current and the 'battery current available' signals are accessed through the CANbus from the battery control module – thus, as long as the control parameters in the control loop are properly adjusted, the battery will always be used in accordance with the battery controller's stated limits. The key is that the control loop compares two values originating from the same control module, via a single current sensor, ensuring that noise and bias error in the measurement is a non-issue. The battery 'current available signal' is computed internally to the battery control module, and is a function of battery state of charge and battery pack temperature according to the manufacturer's proprietary algorithms. Here the fuel cell does not need to be used as an input, as the fuel cell current is controlled independently by the DC/DC converter. The DC/DC converter will also act to shield the fuel cell from overcurrent.

This VTR generation control code was tested using software-in-the-loop validation procedures before being downloaded to the vehicle. These procedures involved developing a vehicle powertrain model, seen in figure 6-10, based on vehicle drag, motor efficiency, the polarization curves of the battery and fuel cell, and the transient performance of all the components. The model code can be viewed in Appendix B.

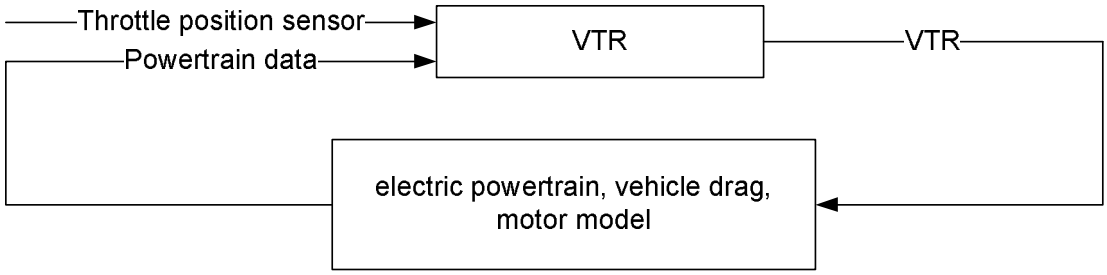

Figure 6-10: Vehicle and powertrain model used to validate vehicle torque request algorithm and ensure powertrain safety

Figure 6-11 shows the impact of the battery control loop on the system from three separate simulations. In these simulations, the vehicle is undergoing wide-open-throttle (WOT) acceleration from standstill, and the fuel cell delivers full power. The simulation was computed in three identical trials, differing only by a change in the 'battery current allowed' value. During the 40kw and 55kw power limit set on the battery, the battery current control loop is active and regulates the current to its maximum – 163 and 251 amps respectively. This is achieved by reducing the total torque requested from the motors. There is also a curve illustrating the battery current that would result if the battery current control was disabled – in this case, the motors draw their maximum possible current. Clearly, the motors are oversized, and power is limited by the amount of available electrical power. The graph also demonstrates the need for a mechanism that will limit the torque to protect the battery pack from overload.

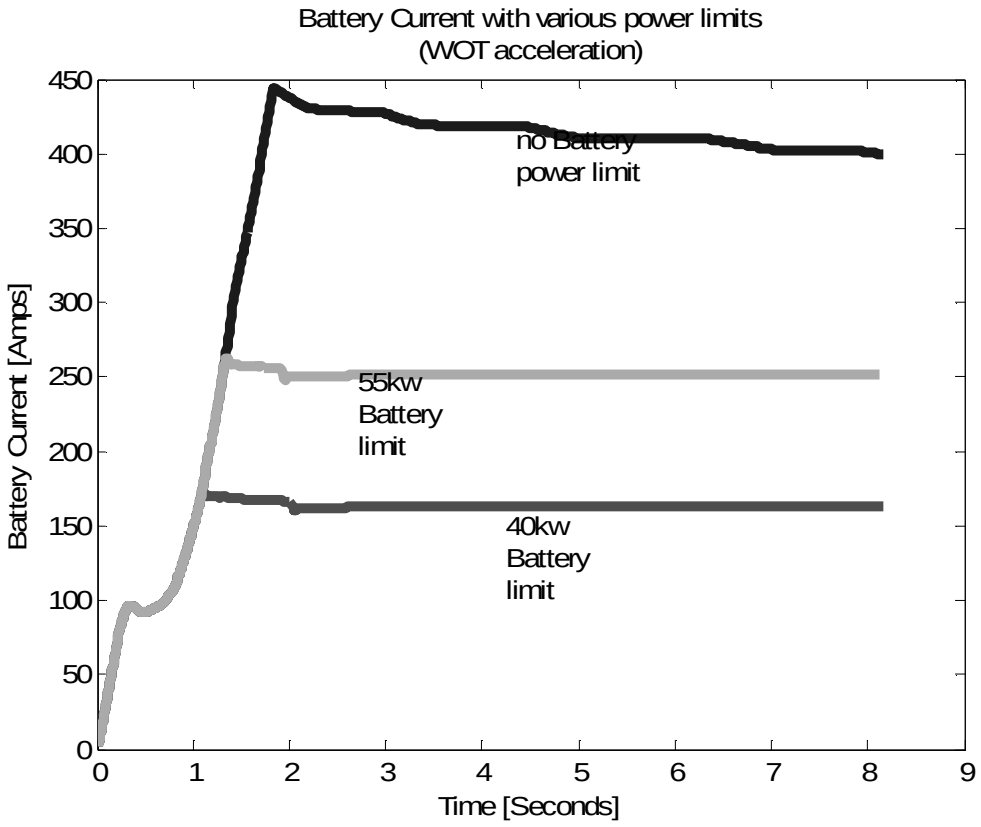

Figure 6-11: The impact of differing battery power limits on a 0-100kph acceleration run.

Although this VTR code is devised to deliver maximum power from the battery at high throttle depressions, it doesn't prejudice the source of the electrical power. During moderate and low power demands, the fuel cell is designed to deliver the needed electrical power. In fact, the fuel cell has its own control loop that (nominally) attempts to drive the battery current to zero. This code was developed by the author concurrently with the VTR code. That particular control loop is not covered under the scope of this work, however can be found for reference in Appendix C.

6.4.2 Torque splitting

The torque splitting scheme is simple. It consists of a lookup table which takes as inputs motor speed and VTR, and generates torque values to be sent to the front and the rear motors. How to generate values to fill this lookup table is discussed in detail in section 6.6.

6.4.3 Traction Control

The traction control scheme that was devised works similarly to a viscous coupling that is commonly found in transfer cases in lower-end four wheel drive vehicles. In an AWD vehicle using a viscous coupling, little or no torque is transferred to the rear axle under normal operating conditions. However, if a speed difference is detected, (for example if the front wheels begin to slip on a low friction surface) then torque is transferred to the rear wheels as a results of the speed difference.

In the present case, differences in motor speeds are detected by the software running on the vehicle microcontroller, and torque is vectored in such a manner to transfer the load to the vehicles with better traction – the slower of the two axles.

The general algorithm implemented in the vehicle is inactive until the speed difference between the two motors is greater than some lower limit. During the simulation of this code, this value was set to 1000 rpm (11 kph wheel speed) at the advisement of GM engineers. At this point, the traction controller will push the torque split in such a way to reduce the difference in speed between the axles.

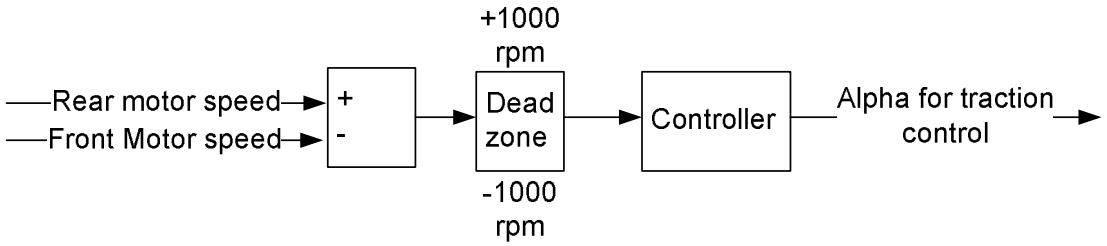

Figure 6-12: The Traction control algorithm

The output of the traction control block is the value alpha, which is defined as the ratio of the desired torque split below:

α = Torque_rear/Torque_vehicle,

Torque_vehicle = Torque_rear + Torque_front

The range of alpha is between 0 and 1, 0 yielding a front-wheel drive vehicle, and 1 yielding a rear-wheel drive vehicle. The alpha value generated by the traction control algorithm is input to the torque arbitration block, where a decision making apparatus (in this case, a simple smoothing

function) arbitrates between the traction and efficiency algorithms. The exact implementation of this code may be found in Appendix D.

This code was simulated with the aid of a wheel slip simulator. This simulator was designed to represent the fuel cell Equinox characteristics, and used a Fiala tire model to characterize tire slip[49]. The coefficient of friction of the tire/road interface for this simulation was trialed with a multitude of values, however the results presented below have it set to 0.5.

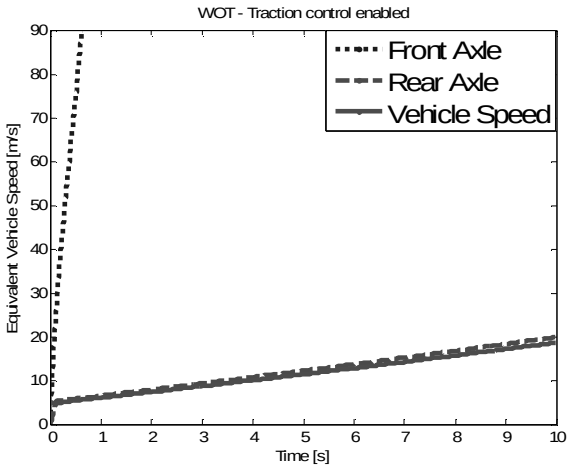

Figure 6-13: Front Axle slipping simulation

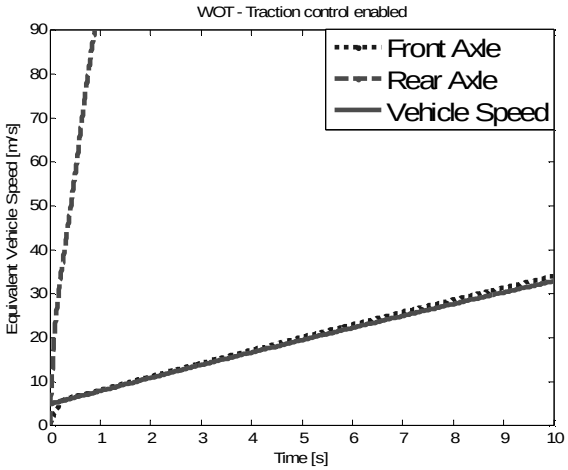

Figure 6-14: Rear Axle slipping simulation

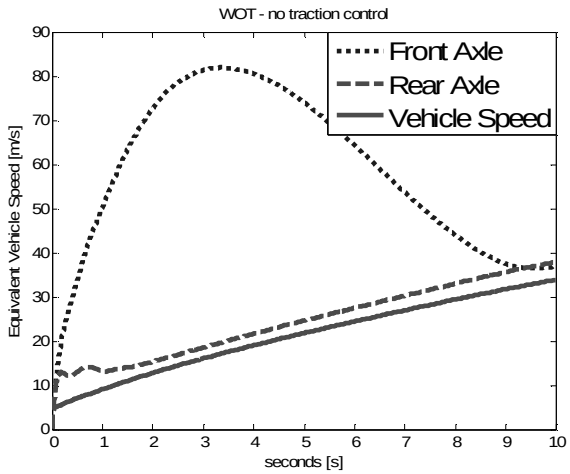

Figure 6-15: Torque split 50/50 front-to-rear

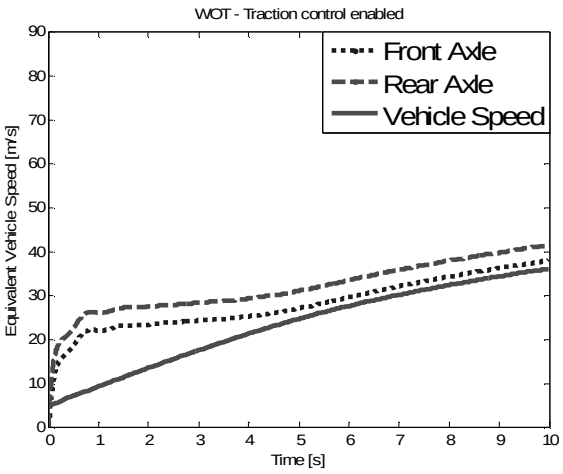

Figure 6-15: Traction Control Enabled

Figure 6-13 and figure 6-14 show the impact of having the front and rear motor respectively produce maximum torque. Each axle respectively is slipping at a very high rate. Figure 6-15

shows the impact of having no traction control system; splitting the torque evenly between the two motors causes the front motor to have high slippage, while the rear motor maintains road contact. Figure 6-16 illustrates the impact of enabling the traction control system: wheel slip is controlled to manageable levels, and the vehicle produces a higher maximum speed than any other case – in this case 3 kph faster than the next fastest (50/50 torque split: 33 kph vs. traction control: 36 kph).

6.4.4 Torque Arbitration

Upon the traction control system becoming active, there is a need to smoothly blend the transition of torque from the efficiency-based torque split to the traction control-based torque split. This is done in order to avoid harsh transients that might be caused by abrupt switching of the alpha-value. This can be implemented by smoothly, linearly ramping the efficiency-based split value to the traction control split value for the duration of the slip event. Once the traction control system manages to equalize the axle speeds, the system will deactivate and the efficiency-based split will attempt to reassert until the difference in axle speeds becomes greater than allowed again, causing the traction system to again take over control of the torque split. This will continue until there is no need for the traction system to activate and the vehicle will resume using the efficiency-based method. The specific smoothing rates that are applied to this transition need to be tuned in-vehicle in order to reduce vehicle jerk. The motors do have an internal response time of 50 milliseconds, which will smooth very fast changes in torque, however, perhaps not enough to produce adequate drivability.

6.5 Torque Splitting

There are three possible algorithms proposed to split the VTR into torque commands for each motor:

1. 50/50 constant split – the VTR is always split exactly in half and requested from the front and rear motors;
2. overflow method – The VTR is requested from a single motor while that motor can provide the entire VTR. If a single motor cannot provide the VTR, the residual is provided by the second motor – the torque request *overflows* to the second motor;
3. optimum efficiency method – the VTR is split between the two motors according to some pre-computed method that attempts to minimize total electric power consumption by targeting the motor's most efficient operating point.

Central to any discussion of torque splitting is alpha, which defines the ratio of the torque split between the front and the rear (as previously defined in section 6.4.3):

α = Torque_rear/Torque_vehicle,

Torque_vehicle = Torque_rear + Torque_front

All torque split algorithms are simply methods to compute alpha. If alpha is equal to 0, than the front motor generates all the torque. If alpha is equal to 0.5, than both motor contribute equally to the torque delivered. Under normal powertrain operation, the rear motor will never deliver more torque than the front in order to maintain the original understeer characteristics of the vehicle. However in certain instances, the rear motor may deliver the most, or all, of the torque if the front motor encounters faults, or enters a temporary torque reduction mode, or perhaps if the front wheels temporarily lose traction.

The alpha values for each of the three calculation methods are shown in figure group 6-16. The top-left figure shows the 50/50 alpha lookup table (α = 0.5 everywhere), the top-right figure shows the overflow alpha lookup table (a smooth transfer of torque to the rear motor), and the bottom figure shows the optimum alpha lookup table (targeting the max efficiency line seen in figure 6-2).

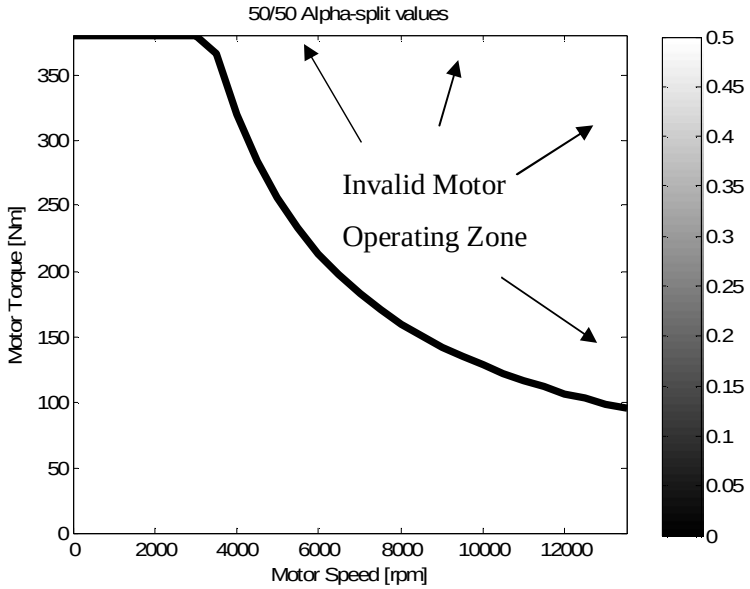

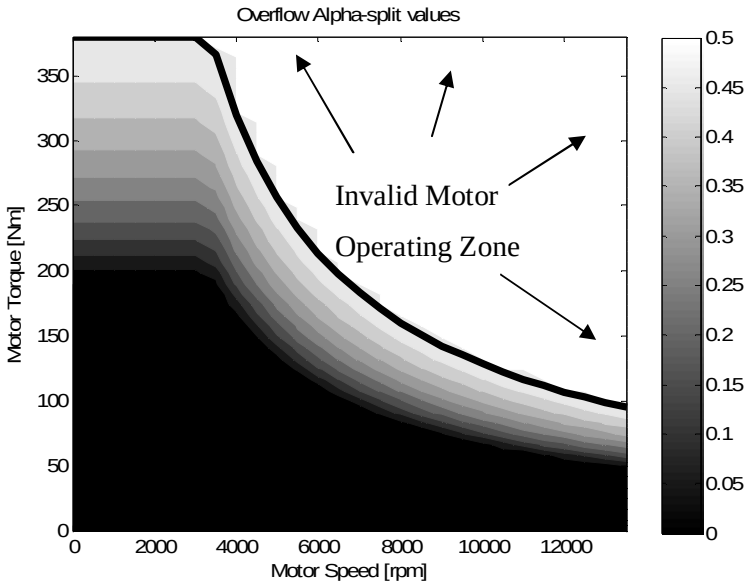

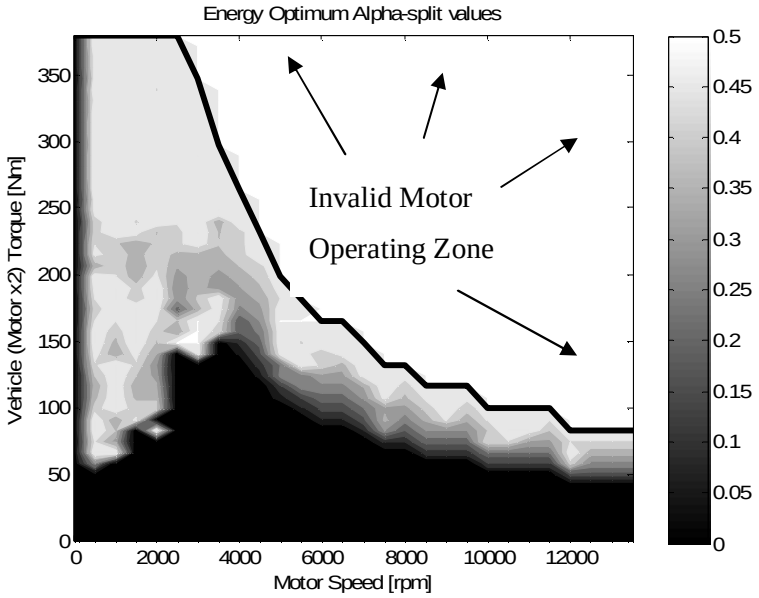

Figures 6-16: Alpha Loop-up tables for the three methods (in-vehicle use). Alpha as a function of speed and Vehicle Torque Request.

6.6 Torque Split Calculation

This section will explain the calculation for the three methods shown in the figures 6-16.

6.6.1 50/50 constant split

This method is algorithmically simple: alpha is simply set to a constant of 0.5.

These alpha values make no attempt to improve efficiency. They will be used as a control, to compare the overflow method and the optimum efficiency method.

6.6.2 Overflow method

This method utilizes the front motor predominantly, until that motor no longer has the torque capabilities to meet the demands of the driver, at which point, the rear motor activates to assist. It calculates alpha using the following equation:

$$\alpha = 1 - \frac{\min(T\max, VTR)}{VTR};$$

where Tmax is the maximum torque that can be delivered at the current motor speed, and VTR is the vehicle-torque request.

This should exhibit increased overall efficiency compared to the 50/50 method due to the reducing time spent at low torque values, as well as increasing the torque load on the motors, which will incidentally move the operating point towards, the maximum efficiency curve of figure 6.2.

6.6.3 Optimum Efficiency Method

The optimum efficiency method should improve total efficiency by reducing the time spent at low torque values, in the same manner that the overflow method did, as well as specifically targeting the maximum efficiency curve of figure 6-2. This algorithm is not trivial, and is detailed below.

Ballard Power Systems Inc. provided steady-state efficiency maps for the ranger motor systems used in the vehicle. This data covered four different bus voltages (250, 300, 350 and 400 VDC), and gave electrical-to-mechanical power efficiencies for the operational space of the motor (10 Nm torque value increments, and 500rpm speed increments).

Since the speed of the vehicle determines the speed of the motors, through a single gear reduction, and this speed changes relatively slowly compared to the computational update period (10msec), the speed of the motor can be considered fixed for that period of time. This assumption simplifies the problem solution to a lookup table which produces the torque split ratio alpha.

Alpha is indexed from a lookup table using motor speed and vehicle torque request. It is then used to generate the front and rear motor torque values using the above equations. Refer to Appendix E for implementation code.

Generating the alpha values to fill the lookup table is pre-computed using a custom optimization routine coded in Matlab. This routine implements an exhaustive search method to find the optimum torque split between motors at each operation point. This algorithm is explained below, and the complete code can be found in Appendix F:

For each operating point of the motor (speed and torque), perform the following:

1. Restrict alpha to that which is feasible based upon whether a single motor can deliver the vehicle torque request (VTR). eg. If VTR > maximum torque from one motor, then alpha must be greater than 0. Also, alpha cannot be greater than 0.5 - since we use two identical motors, alpha is symmetrical around 0.5.
2. Split the feasible alpha range into 0.01 sized intervals.
3. Calculate the front and rear torque based on each of these alpha values.
4. Use the efficiency tables (and the current motor operating point) to calculate the motor efficiency for each alpha value.
5. Calculate the total power entering each motor using the operating point and the efficiency of each motor for each alpha value.
6. Sum the power consumption of the front and rear motor for each alpha value.
7. Find the alpha value that corresponds to the smallest power consumption.
8. Output this alpha value to be saved into the lookup table.

This algorithm produces expected results: At low speeds and medium VTR's, alpha increases from zero in order to keep the torque delivered by each motor from reaching peak values, this can be seen labeled as the 'zone of interest'. This improves the total efficiency. At high VTR's, regardless of speed, alpha is forced to 0.5 as it runs into the torque limits of the motors. Other than these two areas, the alpha values are 0.

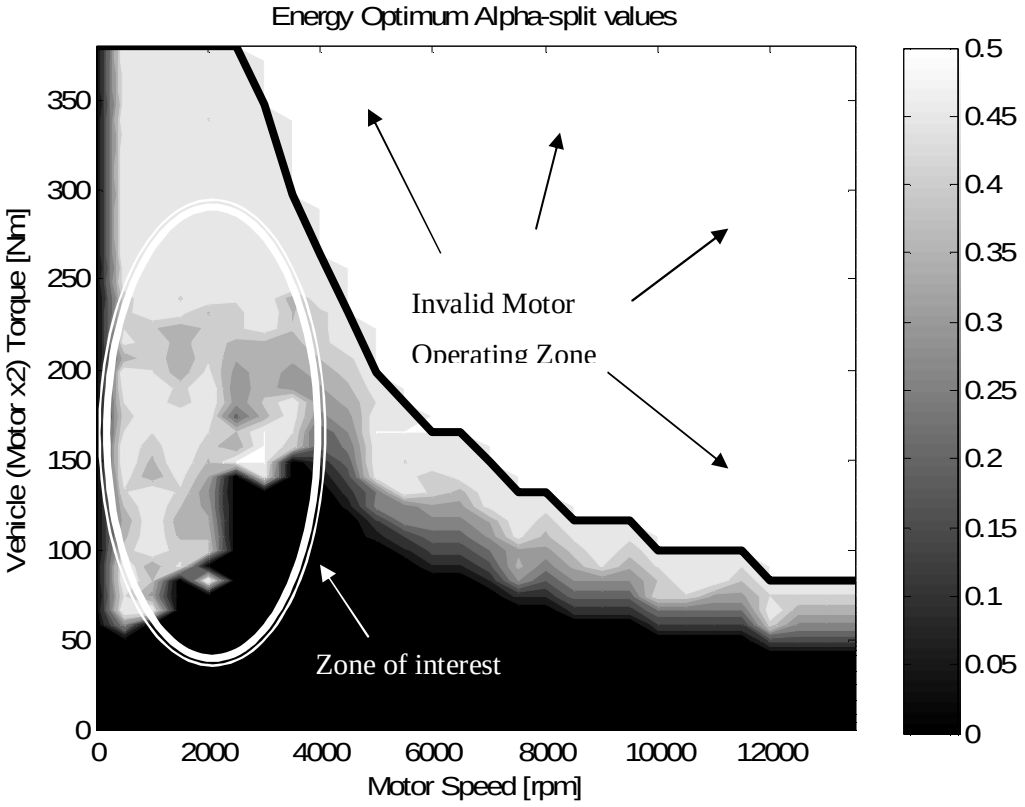

Figure 6-17: The alpha lookup table for the optimum method

The zone of interest is of special note since this is the sole, and key, distinction from the overflow method. It is when the vehicle operates in this area that this method of generating alpha outperforms the overflow method – the maximum efficiency curve is being targeted. This will be seen in the next section.

6.7 Vehicle Simulation

Before implementing these alpha-generation methods into the vehicle, it was necessary to estimate the impact of these methods with respect to:

- the total vehicle efficiency (ie. will it be significantly affected by simply switching torque-splitting methods); and
- the feasibility of detecting changes in the vehicle's overall efficiency when switching from one method to another.

This impact estimation was performed using a vehicle model generated within Simulink and which had been previously validated using the stock Equinox model. This vehicle model accepted as input any arbitrary drive cycle. The model proceeded to calculate the total forces on the vehicle resulting from rolling resistance, aerodynamic drag and acceleration forces. The model then transformed these forces (and the instantaneous speed of the vehicle) on the motor rotor, to calculate the torque and speed of the rotor needed to meet the drive cycle – negative torques are ignored for the purpose of simplicity. The rotor torque was split according to the torque split lookup table, and the efficiency of both motors were referenced from lookup tables, and the total electrical power required was calculated. By integrating the power over the drive cycle, the total electrical energy consumed was obtained. This model was simulated three times, once for each alpha-generation method, and the total energy consumed during each simulation was compared. The model only examined positive (motoring) torques. That is, regenerative braking is not in use, this is done for simplicity. Neglecting regenerative braking should not have any effect on the final results, as the total efficiency will merely be improved overall by its inclusion, not at specific points in the drive cycle.

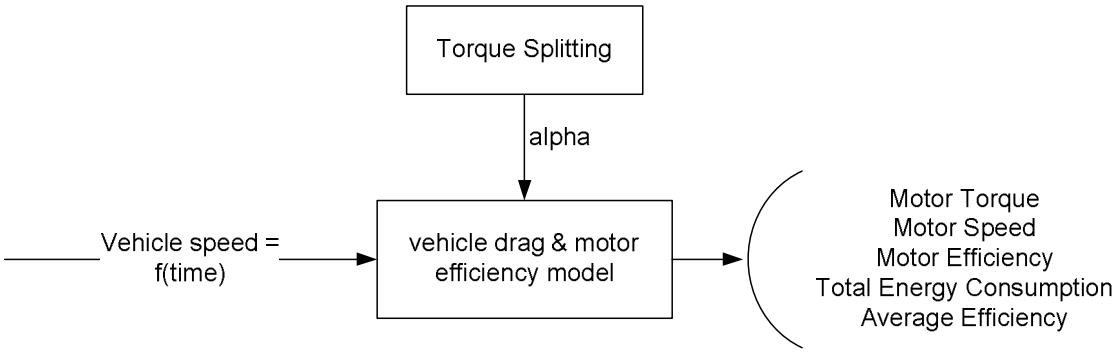

Figure 6-18: The vehicle model used to estimate the impact of different torque splitting strategies.

6.7.1 Vehicle Model

The vehicle-drag model was simple:

$$F_{drag} = F_{aero} + F_{rollingdrag} + F_{grade} + F_{accel}$$
$$F_{drag}(t) = 1/2\rho v(t)^2 C_d A_{frontal} + C_{roll} mg + 0 + ma(t)$$

where ρ = air density, v(t) = vehicle velocity as function of time (the drive cycle), C_d = coefficient of aerodynamic drag (0.417 for the Equinox), C_{roll} = coefficient of rolling drag (0.009 for the tires to be used), $A_{frontal}$ = frontal area of the vehicle (2.686 for the Equinox), m = vehicle mass (2300kg for the Fuel Cell Equinox), g = gravitational constant (9.8), a(t) = vehicle acceleration as a function of time (the derivative of drive cycle).

The model validation, which was presented in previous work[50], can be viewed in Appendix G.

6.7.2 Torque split algorithm simulation results

Simulations were run on six distinct drive cycles in order to evaluate the impact of each torque splitting method with respect to various drive cycles. Drive cycles[51] were chosen to represent a variety of conditions, and included:

FTP75 – urban drive cycle

US06 – aggressive driving cycle (urban/highway)

REP05 – aggressive driving cycle (highway with spurts of heavy traffic)

HL07 – aggressive engineering test cycle (intended for emissions testing)

Custom 1 – Stoplight-to-Stoplight (0.3 km distance, max speed 72 kph)

Custom 2 - Moderate acceleration (1/2 throttle, 0-90kph)

All drive cycles profiles can be seen in Appendix H.

6.7.2.1 Energy consumption comparison

The simulations show significant improvements between the different torque splitting techniques. Figures 6-19 show the total electrical energy consumption for each technique on the six distinct drive cycles. This is the electrical energy consumed by the motors in order to propel the vehicle through the specified drive cycle.

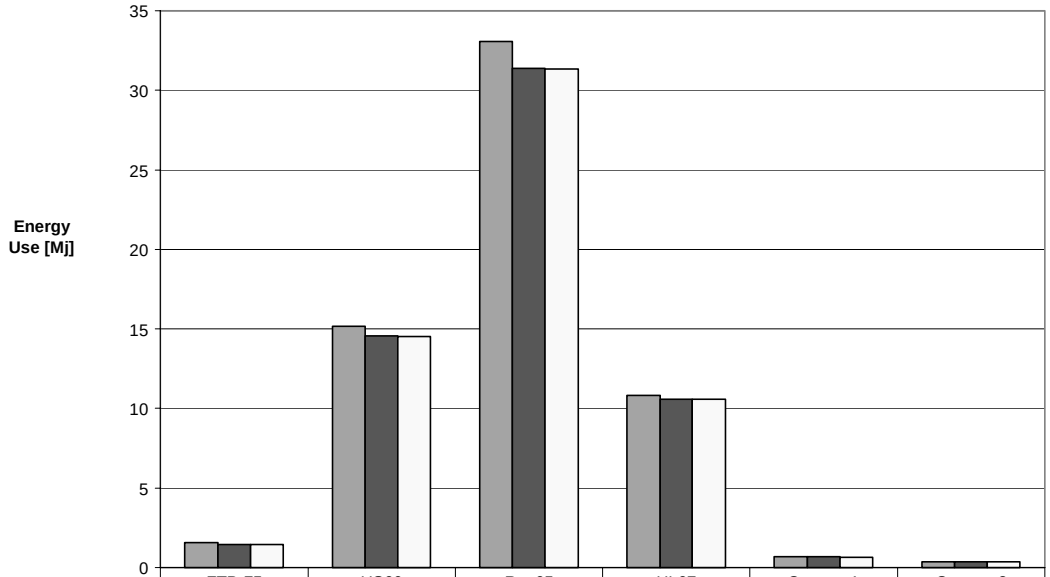

	FTP-75	US06	Rep05	HL07	Custom 1	Custom 2
50/50	1.58198	15.175	33.0565	10.8171	0.67702	0.378033
Overflow	1.46192	14.5662	31.3532	10.5722	0.668089	0.382721
Optimum	1.46065	14.5482	31.334	10.5664	0.662778	0.377412

Figure 6-19: Total Electrical energy use during various drive cycles by each torque-split strategy

6.7.2.2 Energy consumption comparison (percentage difference)

A better indicator than total electrical energy used is the percentage difference of energy expended between the different torque-split methods. These results can be seen in figure 6-20. In this figure, the 50/50 torque split is used to compare the overflow and the optimum methods. The percentage difference is calculated as the amount the latter two cases outperform the 50/50 split. Clearly, simply moving away from the 50/50 torque-split method generates large benefits in most cases. There are smaller benefits to moving from the overflow method to the optimum method, however the optimum guarantees that the maximum possible efficiency is achieved, which can be seen the ‘custom 2’ drive

cycle, where the overflow method actually performs worse than the 50/50 method, yet the optimum method outperforms both.

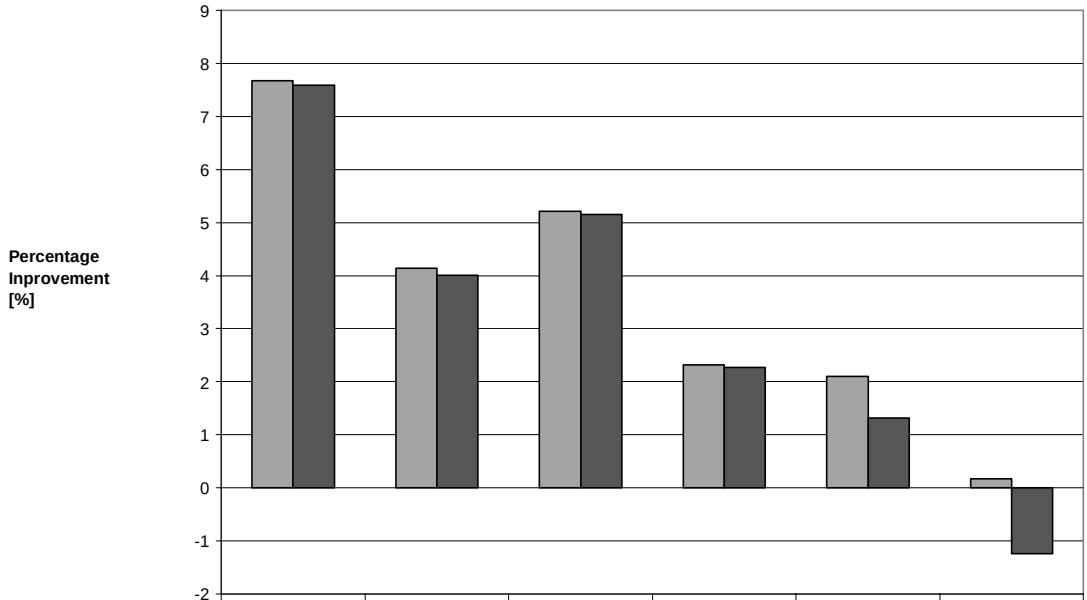

	FTP-75	US06	Rep05	HL07	Custom 1	Custom 2
Optimum vs. 50/50	7.669502775	4.130477759	5.21077549	2.317626721	2.103630617	0.164271373
Overflow vs. 50/50	7.589223631	4.011861614	5.152693116	2.264007913	1.319163393	-1.240103377

Figure 6-20: The electric energy consumption (percentage difference) comparing the 50/50 method to the optimum and overflow methods

6.7.3 Explanation of simulation results

There are two immediate questions that arise from the above results:

- Why does the 50/50 method produce such sub-par efficiency compared to the optimum and the overflow methods?; and
- Why do the simulation results show such high levels of dependency on the specific drive cycle? And if such high levels of dependency on the drive cycle exist, how do we assess the true benefit to upgrading the control strategy?

The main reason for the low relative efficiencies of the 50/50 method arises due the motor efficiency behavior as the motor approaches zero torque or speed: efficiency approaches zero. If, for example, the vehicle spends more time at low speeds or torques (less then 500rpm or 10 Nm), then the efficiency of the motor during these periods will be very low. This is shown in figure 6-21. as the

area of interest. The main benefit of the overflow and the optimum method over the 50/50 split method is that they attempt to maximize the torque one motor produces, and minimize the time the motors spend in this region of low efficiency. The other reason is that, in general, the efficiency increases with respect to torque (regardless of speed). Thus, by reducing the torque both motors are producing will, in general, reduce the total efficiency.

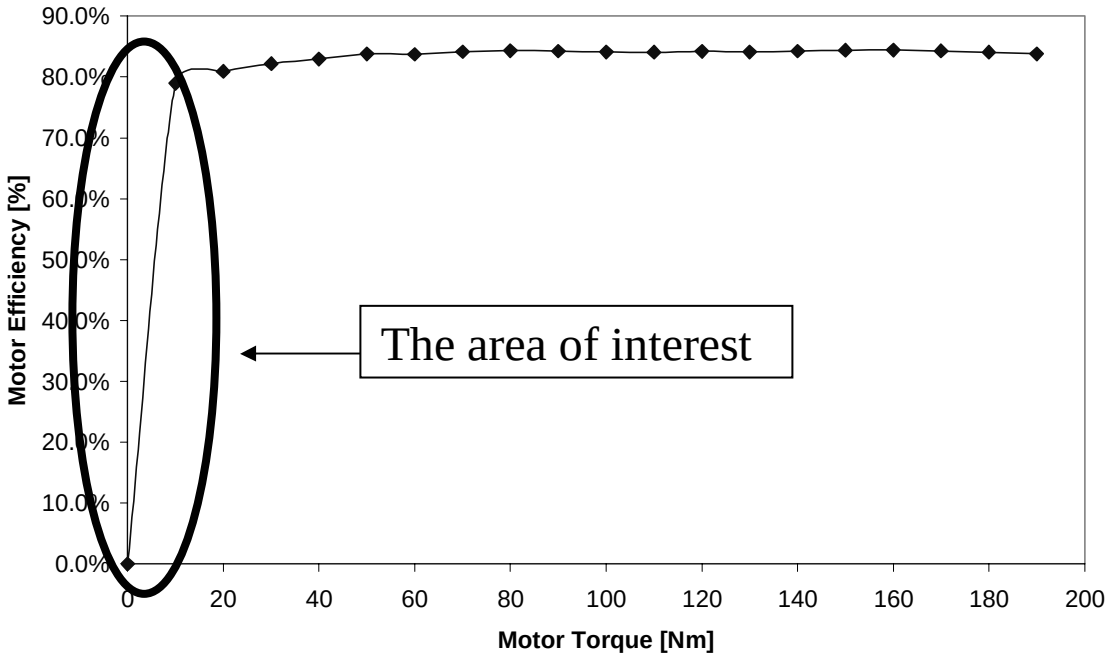

Figure 6-21: Motor Torque vs. Efficiency at 2500 rpm

Also important to note is that the simulation does not fully account for the steady-state load that the motor inverter draws while on. This load is accounted for by the motor efficiency maps while the motor is drawing load, but is not while the motor efficiency is 0%. This load has been measured at 150 Watts. This load, if accounted for would further skew the efficiency gains away from the 50/50 torque splitting method, since the overflow and optimum methods could make further improvements by shutting down the inverter that is not being used. The restart time of the motor may preclude this option from being used aggressively – this will depend highly on the drive cycle.

The dependency on the specific drive cycle is another important facet. The drive cycle, along with the vehicle mass and drag coefficients, directly determines the operating point of the motors. Figure 6-22 and figure 6-23 shows the results of using the drag vehicle characteristics to transform the vehicle speed from a vehicle-specific drive cycle into the motors operating region and overlaying that on the motor efficiency map. Each point represents the motors operating at that torque and speed for 0.1 seconds. It is clear that these two drive cycles are placing different demands on the motors.

The FTP cycle is a relatively low-torque, low speed demand characteristic of urban driving. The US06 drive cycle places much higher load on the motors and operates at higher speeds.

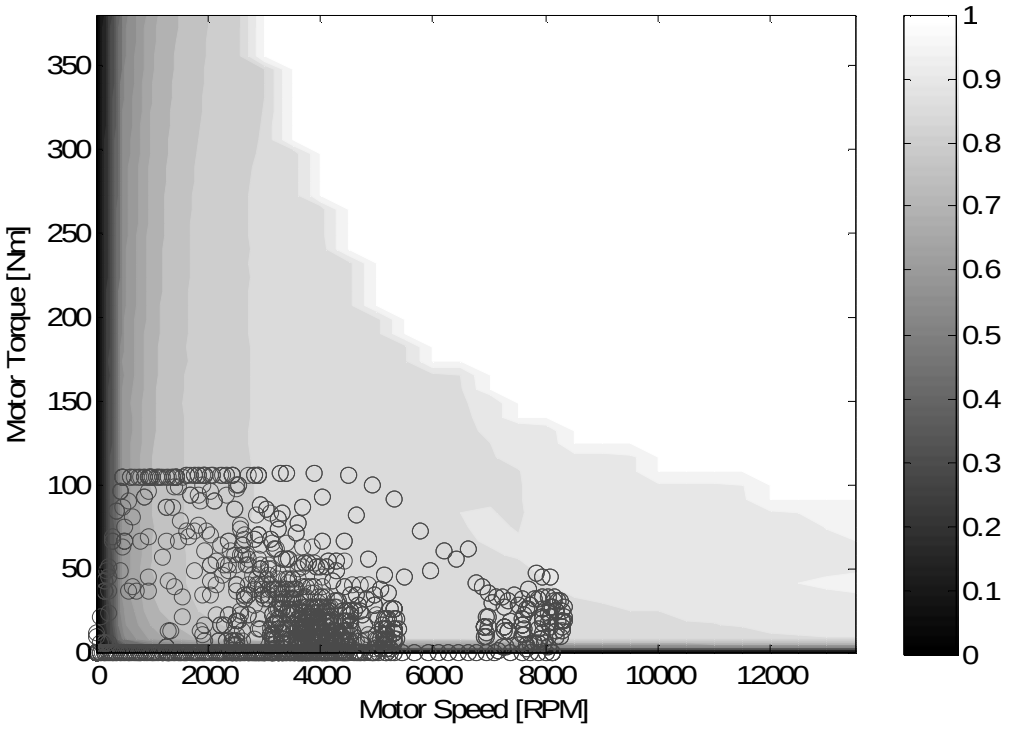

Figure 6-22: Optimum alpha efficiency map overlaid with FTP-75 motor operating points

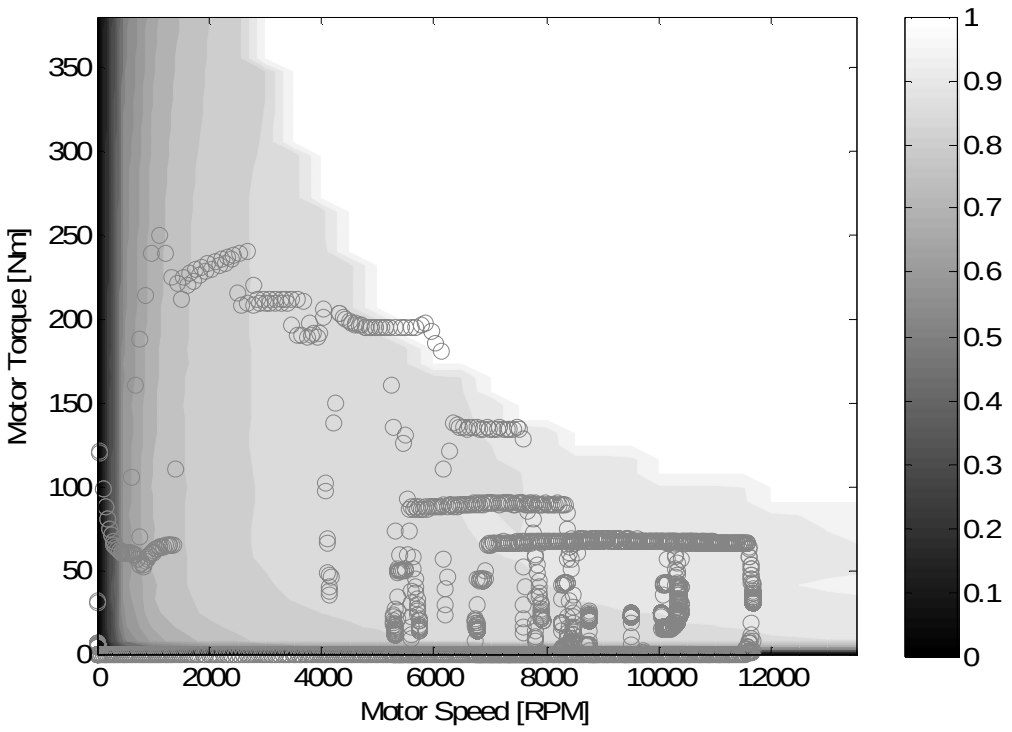

Figure 6-23: Optimum alpha efficiency map overlaid with US06 motor operating points

As always, determining the impact of specific control modifications must be done within the context of the drive cycle. A lack of good driving cycle data impedes the real-world estimates of the efficiency improvements. Here, the drive cycles used were chosen as best representations of real-world driving behavior. However driving patterns are influenced by a wide variety of factors including: driver age, vehicle age, time of day, weather, etc. Truly determining the energy impact of these strategies is impossible, as the real-world driving patterns are unknown; the best analytical technique available is to use the same drive cycles that the automotive manufacturers, and the U.S. EPA use for fuel economy and emissions testing.

Chapter 7
Conclusions and Recommendations

7.1 Conclusions

A method for generating vehicle torque requests, performing simple traction control, and implementing several torque split strategies has been presented and simulation results have been shown. This code forms the core of what seems to be a competent torque control strategy, and can be used directly in AWD electric vehicles. Porting of this code to different vehicles and different electric vehicle types can be accomplished by modifying the relevant parameters of each block of code.

The vehicle torque request code produces good results based on the simulation. Since the vehicle power is limited by the total electric power available on the vehicle (the motors are rated for more power than the battery and fuel cell combined), there is a need for overcurrent protection for these components. This is accomplished via a feedback control loop that activates when the battery current gets dangerously high; the battery controller determines what the current limits of the battery are as a function of state of charge and temperature. While this feedback control loop is not activated, the throttle pedal linearly controls the total torque available from the motors. The simulations show full, linear delivery of torque to the driver up to the limits of the powertrain.

The traction control simulations indicate that using an *'axle-speed equalization' type of control is feasible*; the system splits the torque in such a way to keep the front and rear motor rotors moving at the same speed (within 1000 rpm of each other). This control will need to be tuned in the vehicle to produce the time response and to verify an appropriate amount of wheel slip. This control can also be used as a base upon which to further expand the functionality of the traction control system. How specifically this can be done will be discussed in the recommendations section.

The energy efficiency simulations show a clear advantage to using an intelligent torque-splitting strategy. Three different strategies are presented, a 50/50 split method, an overflow split method, and an optimum split method. *Simulations indicate a greater than 7% gain in efficiency* is achievable during the FTP75 drive cycle, by using the overflow method, or the optimum split method instead of the 50/50 split method. Lesser, but still very significant gains in efficiency are apparent on the other drive cycles. These results must be validated further with either road testing, or more in-depth testing of the motors on a dynamometer. In particular, motor efficiency at very low torque and speed values must be better defined. This issue will be further discussed in the recommendations section.

7.2 Recommendations

There are a number of items and issues that need to be further addressed before the impact of the torque split strategies are definitively determined, and the entire torque control strategy can be implemented into the vehicle. The next three sub-sections will discuss how this work can be carried forward, and will make specific recommendations on what should be done before implementation into the vehicle, and what work could be performed in order to upgrade the code.

7.2.1 Vehicle Torque Request

The vehicle torque request transients must be experimentally determined in-vehicle. Specifically, the over-current protection that the feedback loop provides the battery takes time to activate; it is conceivable that this speed of activation is not fast enough to always maintain the battery current below the maximum. There are a variety of parameters that are not well enough understood to accurately predict the needed response of this control loop pre-installation into the vehicle, including the transient response of the motors, transient internal battery resistances, and the rate of change of the maximum current limit. It is recommended that the vehicle torque request be implemented as is into the vehicle, and the controller is further programmed to trigger a fault upon the violation of the battery limits. Then, the activation point of the control loop can be tuned to eliminate these faults.

There may also be a need to limit motor torque in order to keep the motor voltage from dropping below the required input voltage of the motor, which may fault the motor controller. This need may increase as the battery begins to degrade, and its internal resistance increases. It is recommended that the over-current control loop be used as an example to produce the voltage controller. The loop should become active at some low voltage, and regulate the vehicle torque request in order to keep the battery voltage above the minimum level.

7.2.2 Traction control system

The traction control code illustrated in this work is a very simple type of traction control, acting only to ensure that the front and the rear axles are slipping the same amount. This relies on the driver to reduce the total amount of torque if both axles are slipping too aggressively. Further, it does not address the issues related to the limited-slip differential – if only one wheel on the front slips, this will limit the amount of torque that could be applied to the other wheel on the front.

An accelerometer should be used to deduce actual vehicle speed (integrating, combined by periodic on-motion recalibrations using non-driven wheel speeds). This vehicle speed should then be used to set targets for the motor axle speeds. This will place the motors under closed loop speed control while the traction control system is active, and will allow their speeds to be set such that their tire slip is optimum for maximum acceleration. This could act as a second stage of traction control, beyond the simple 'axle-speed equalization' control. This is a fairly straightforward design. However it will require a significant amount of testing and tuning to obtain a well-performing system. It allows automatic traction control, requiring no extraordinary driver skill.

Implementing an even more complicated traction control system that allows correction for an axle that encounters mixed-friction surfaces requires special hardware to apply braking torque to the wheel that is on the lower friction surface. This can be accomplished via an electronic brake controller that allows independent brake line pressurization without activation of the brake pedal. This is extremely complicated and requires a large investment in time, energy, and resources.

7.2.3 Torque Splitting Algorithms

The simulations currently show significant gains in energy efficiency are possible by simply choosing an appropriate method of splitting the torque between the front and rear motors. In order to prove the validity of these simulations, the vehicle must be run on a dynamometer using the different torque control strategies, and the electrical consumption must be measured accurately. Alternatively, the motors may be tested in the operation regions that produce the most efficiency gain, in order to improve resolution, and improve the simulation. This requires testing at low torques and low speeds, and accurately measuring speed, torque, current and voltage. In order to do this, the motor should be arranged such that both outputs of the differential drive a single shaft, which delivers torque to a dynamometer load. The current should be calculated by measuring the voltage across a high power resistor in line with the motor in order to improve accuracy.

Assuming that the optimum efficiency method is found to have the best efficiency in-situ, *there is a need to evaluate the impact of the torque-splitting algorithm on stability and drivability.* The transfer of torque may cause discomfort, or driver startle in certain instances. This impact must be evaluated on a closed track before release of the code. Additionally, vehicle stability needs to be addressed as well by producing a driving cycle that includes an aggressive lane change. With the torque split enabled, the vehicle should be placed into a situation where torque rapidly transfers to the rear motor, while the vehicle has a high amount of lateral acceleration placed on it. This could also be done on a limited friction surface in order to help find the stability limits of the vehicle.

7.2.4 Application of concepts to the Pacifica configuration

The torque control strategy framework can be improved in order to facilitate implementation into the Pacifica vehicle. The overall four block structure can be maintained, with the addition of a single block to generate throttle position control signals that are needed to control the torque delivery from the engine. Also note that three torque commands must be generated: front motor, rear motor, and engine. The addition of a tertiary torque source precludes the use of alpha – this second degree of freedom in the system necessitates a second variable. Figure 7-1 illustrates the changes needed to implement this system into the Pacifica.

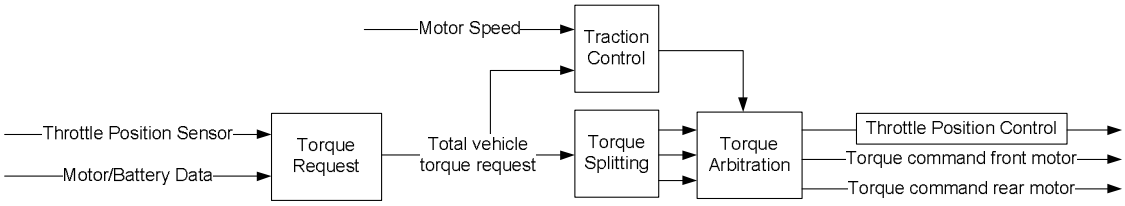

Figure 7-1: A reconfigured torque control strategy framework to implement into the Pacifica

Appendix A

VTR Code for use in-vehicle

VTR Code

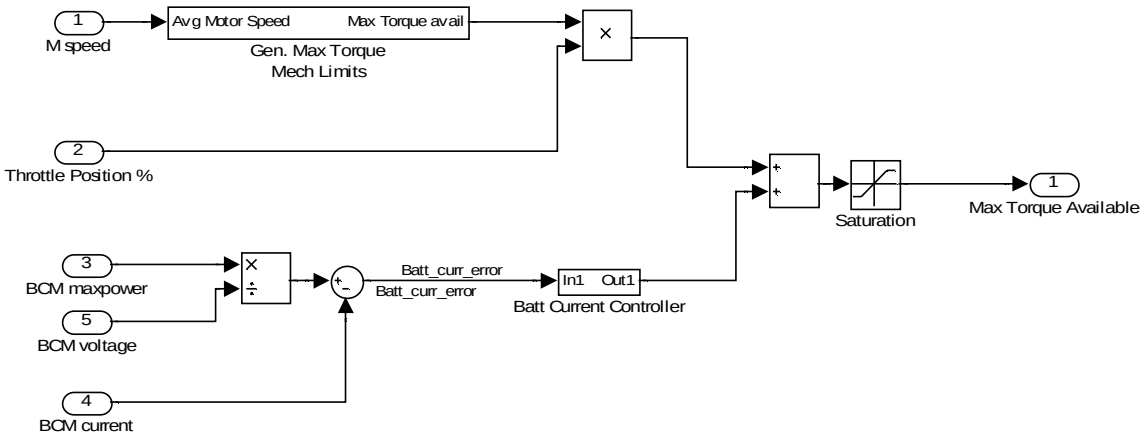

Gen Max Torque Mech Limits Block (see VTR code for context)

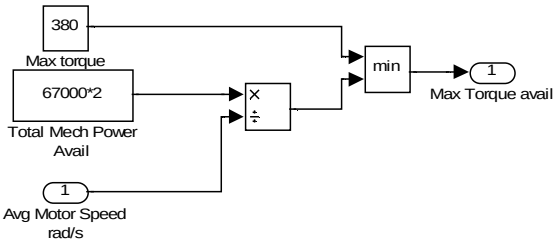

Batt Current Controller (see VTR code for context)

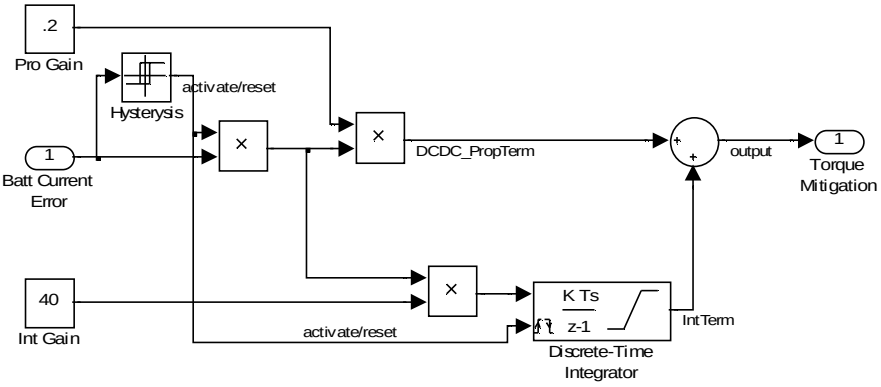

Appendix B

VTR Simulation model code

Software in the loop testing of VTR control code is shown below. The model is controlled using the throttle control gain slider located on the left. The upper three blocks contain the powertrain control code, and the bottom block contains the powertrain model.

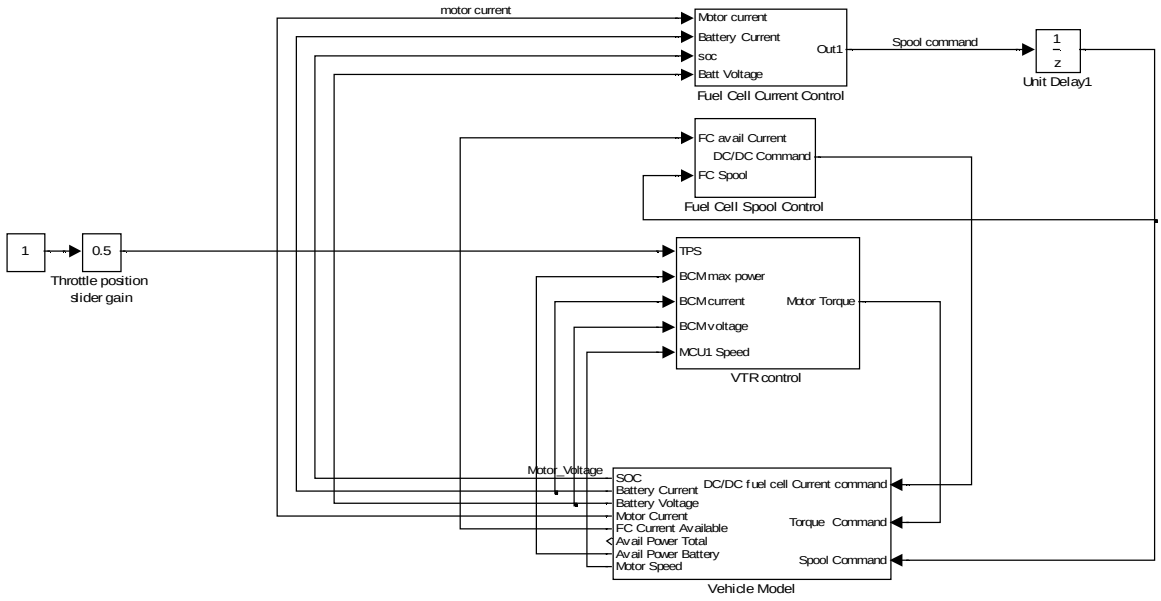

The vehicle model is shown below.

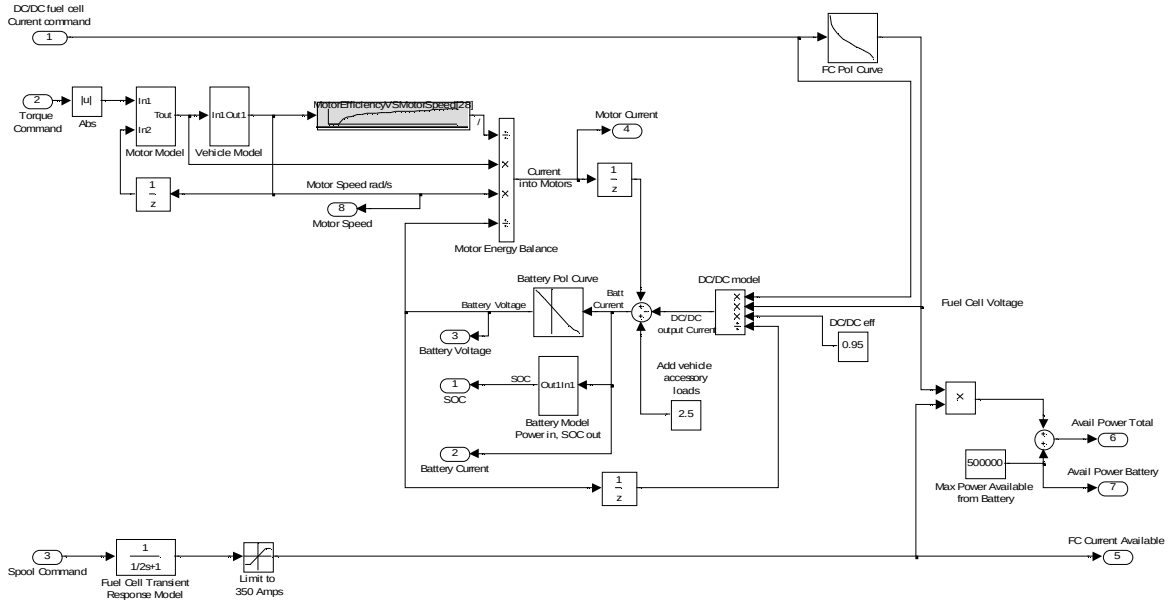

Appendix C

Fuel Cell Current Control Loop

The below code shows the hybrid control strategy implemented to validate the VTR code. It activates the fuel cell only if the motor current is higher than 40 amps, or if the battery is being charged. When the fuel cell is activated, the FC current controller nominally drives the battery current to zero, unless the battery needs to be charged, at which point, the battery current is driven to -80 amps – the nominal battery charge rate. The battery charge rate will be reduced if the battery voltage is rises high enough to potentially cause the motor inverter to shutdown (less than 5 volts from the inverter maximum).

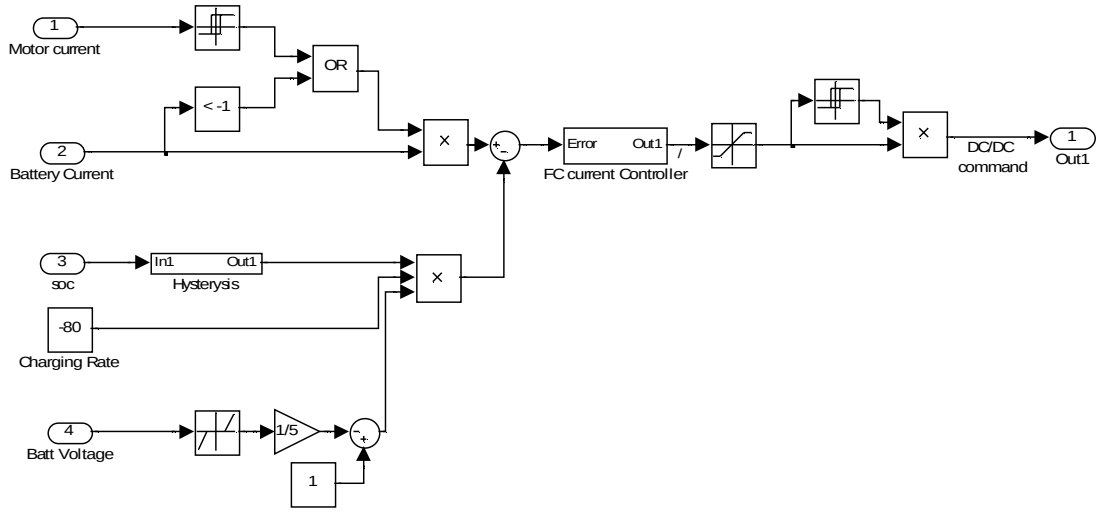

The FC current Controller is a simple PI controller, and is shown below.

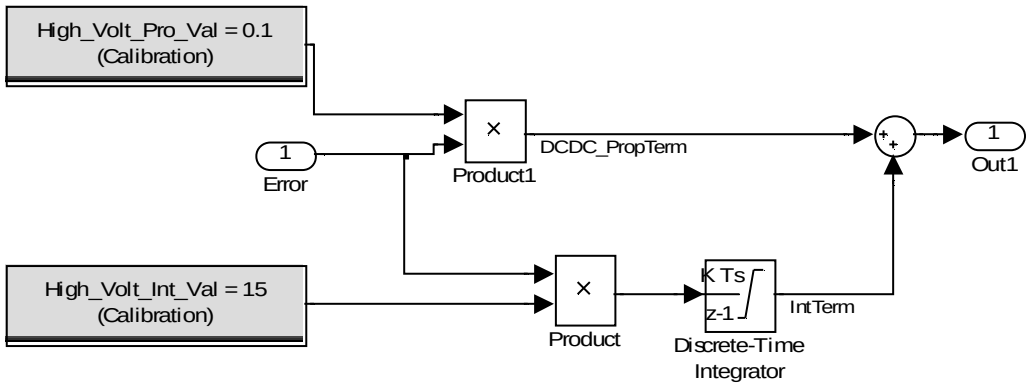

Appendix D

Traction control code

The below code shows the traction control algorithm that is used in-vehicle.

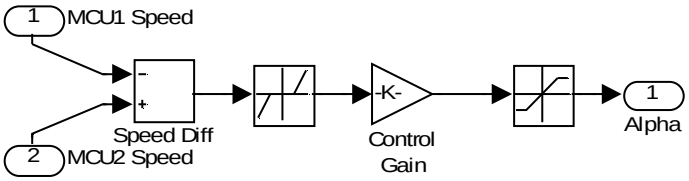

Appendix E

Generating Front/Rear Torque Values

The code shown below accepts alpha values and produces the torque values that are issued to the front and rear motor controllers.

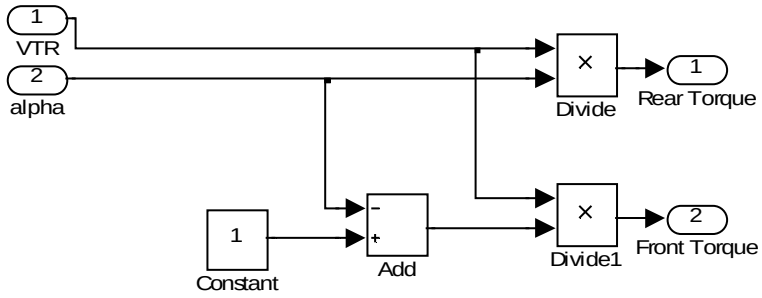

Appendix F

Optimum Torque Split Search Algorithm

```
double Alpha(28,24);
trq_eff_index = [0    10    20    30    40    50    60    70    80    90
      100   110   120   130   140   150   160   170   180   190   200
      210   220   230];
spd_eff_index = [0    500   1000  1500  2000  2500  3000  3500  4000  4500
      5000  5500  6000  6500  7000  7500  8000  8500  9000  9500  10000
      10500 11000 11500 12000 12500 13000 13500];
eff_trq_map = // removed for confidentiality;
eff_trq_map = eff_trq_map';
spd_eff_index = spd_eff_index*2*pi/60;

for Speed1 = 5:5:135
   for T1 = 1:1:46
      % Speed and T have real values (they are the operating point of the
      % vehicle
      Speed = Speed1*100;
      T = T1*10;

      T_max = trq_eff_index(min(find(eff_trq_map(Speed/500 + 1 ,2:end) == 0)));
      if (isempty(T_max) || T_max > T)
         alpha_lower_limit = 0;
      else
         alpha_lower_limit = (T - T_max)/T ;
      end
      if (alpha_lower_limit > 0.5) alpha_lower_limit = 0.5; end
               alpha_upper_limit = 0.5;
      alpha_lower_limit;
```

```
        alpha_test = [alpha_lower_limit:0.01:alpha_upper_limit];

        % Split the operating torque into 100 steps between front and rear
        fr_T = T.*alpha_test;
        rr_T = T.*(1-alpha_test);

        % evaluate the efficiency of each motor at each value of alpha
        eff_fr = interp2(trq_eff_index,spd_eff_index,eff_trq_map,fr_T,Speed);
        eff_rr = interp2(trq_eff_index,spd_eff_index,eff_trq_map,rr_T,Speed);

        eff_rr(find(isnan (eff_rr))) = 0.0001;
        eff_fr(find(isnan (eff_fr))) = 0.0001;
        eff_rr(find(eff_rr == 0)) = 0.0001;
        eff_fr(find(eff_fr == 0)) = 0.0001;

        E_power = (Speed*2*pi/60)*fr_T./eff_fr + (Speed*2*pi/60)*rr_T./eff_rr;
        Eff = (Speed*2*pi/60)*T./E_power;
        temp  = min(alpha_test(find (min(E_power) == E_power)));
        Alpha(Speed1/5,T1) = temp;
        Overall_Eff(Speed1/5,T1) = T*(Speed*2*pi/60)/min(E_power);
    end
end
```

Appendix G
Vehicle Drag Model Validation

This drag model was validated against the stock Chevrolet Equinox early in the vehicle development program. Data was generated by the Equinox on a test track by GM for this purpose. This data was compared with the data generated from the simulation of the vehicle model, and the results for the fuel consumption and engine torque is shown for three different drive cycles in the following tables:

Table G1: Cumulative Fuel Consumption Percentage Error

	Test Data vs. Normal Simulation	**Test Data vs. updated drive cycle Simulation**
UDDS	-5.95%	-4.4923%
505	-4.23%	-2.57%
HWFET	-1.68%	-1.01 %

Table G2: Engine Torque Error (Simulation vs. Actual)

	Error in Engine Torque [Nm] (Mean/Std. Dev)
UDDS	-5.5237 / 21.5769
505	-1.7027 / 24.1518
HWFET	-0.6922 / 17.3935

The first data column of Table H1 shows the percentage error between the simulation and the test data for the total fuel consumed during each drive cycle. The second data column shows the same percentage difference, only the model was simulated using the actual drive cycle from the test run (small differences exist between the drive cycle specification and the test vehicles on road drive cycle).

Table H2 shows the average and standard deviation of the error between the test data and the simulation data for the instantaneous engine torque; the engine torque for the simulation and the test data was compared at each 0.1 second increment.

Although there was no data available that could directly validate the vehicle drag model, the engine torque data (a good measure of vehicle loading) shows a high mean correlation, with the mean difference being only 5.5 Nm at most. In addition, the fuel consumption (another measure of total power consumed by the vehicle) was reasonable, with less than 4.5% error from the test data.

Further, the fuel cell Equinox was outfitted with a CANbus datalogger. The speed profile of the vehicle was input from a random test drive into the model. The model produced the torque profile that would have been necessary in order to produce the inputted speed profile, and this torque profile was than compared to the data-logged torque estimation value produced by the actual motors. The comparison can be seen in Figure H1, the pink (jagged) line represents the torque that the model predicts is needed to meet the speed profile. The blue (smoothed) line represents the estimated rotor torque produced by the motors.

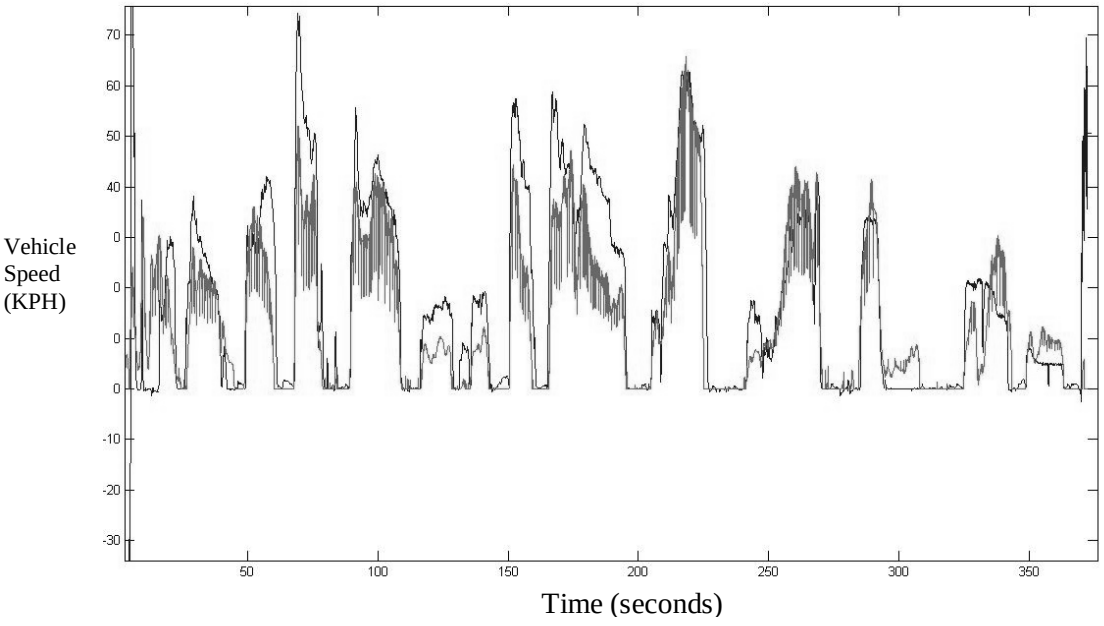

Figure G1. The comparison of the 'torque estimation' value from the motors, and the modeled torque required to meet the drive cycle

There are several reasons that there is some deviation between the actual and the model torque:

- The grade of the test run was not equal to zero – there were unknown gravity loading effects that were not accounted for in the model
- The rotor torque is estimated from the three phase motor currents, and the estimation accuracy relies on its internal motor model accuracy.
- The various losses in the driveline are ignored in the model, including the gear efficiencies
- The model estimates drag using vehicle velocity, which is generated via motor rotor speed. This method of vehicle speed estimation is subject to the bias introduced by tire slip, which is not accounted for in the model.

Even with the above assumption, the deviation for this is still reasonable. The average torque difference between actual and simulated is -3 Nm, and the standard deviation is 16.24 Nm. This is reasonable compared to the simulation/test data comparison done in UWAFT's ChallengeX year 1, Report 1[50]. There, the UDDS (an urban drive cycle) resulted in -5.5/21.57Nm. The increase in accuracy is due to the better quantification of the electric drivetrain, and the ease of modeling such a system compared to the multi-physics complexity of an IC engine.

Appendix H

Common Drive Cycles

Rep05 cycle

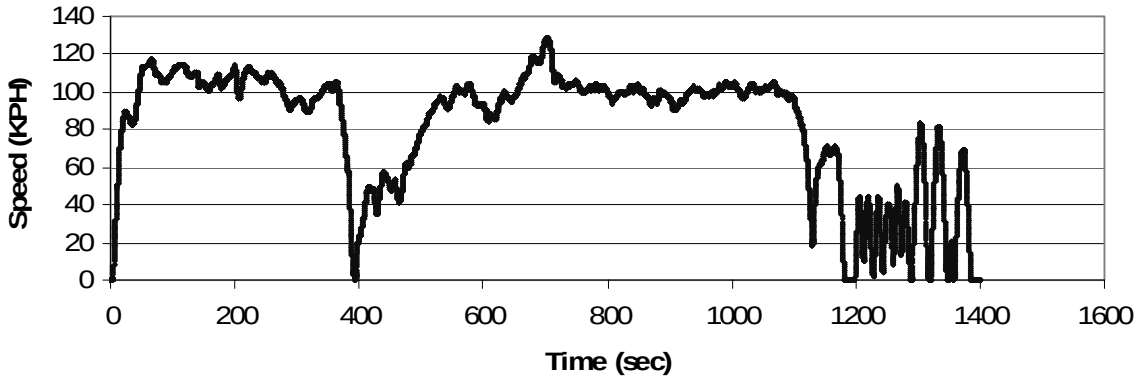

US06

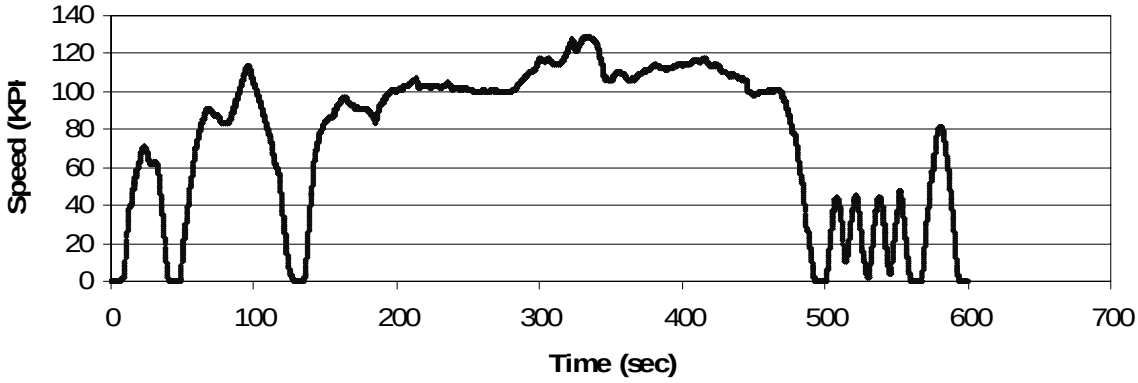

HL07

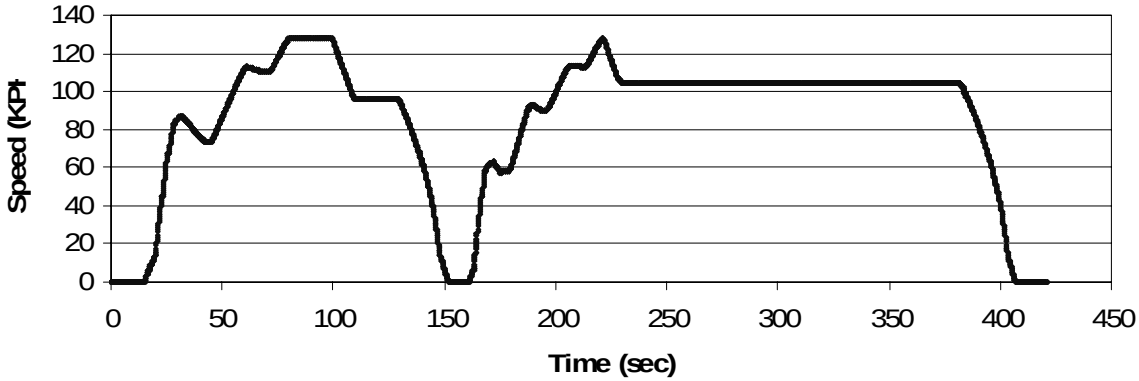

FTP

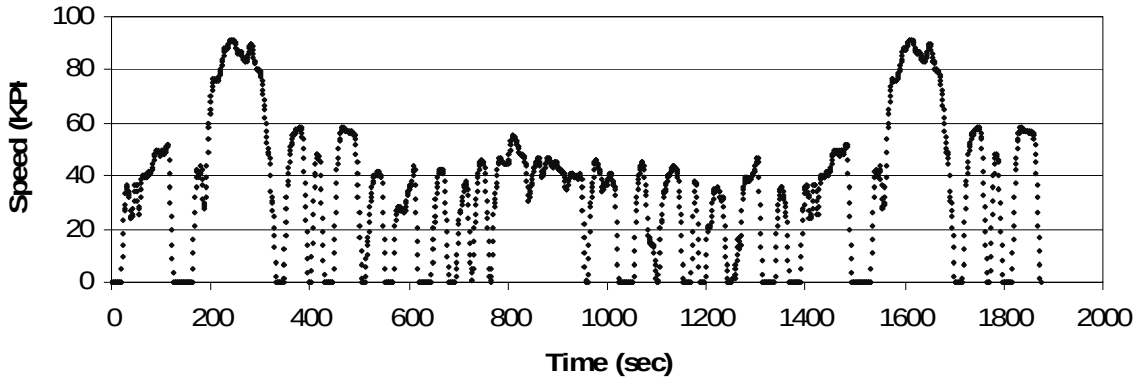

Custom 1

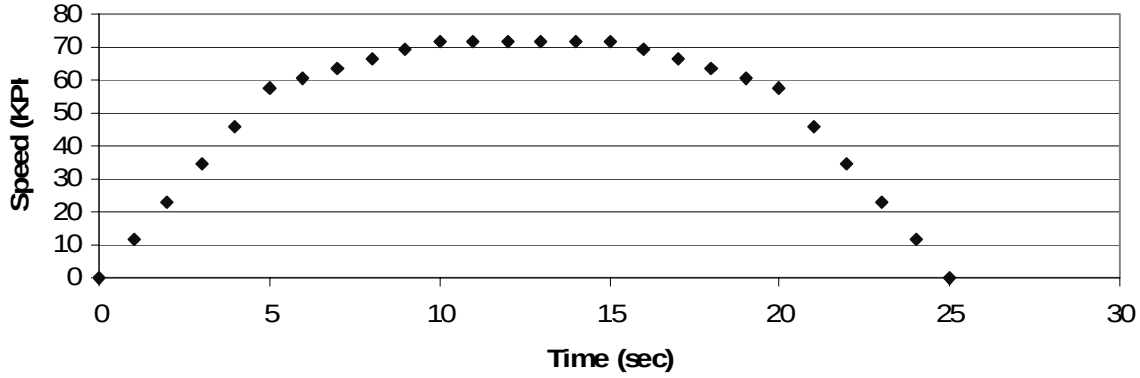

Custom 2

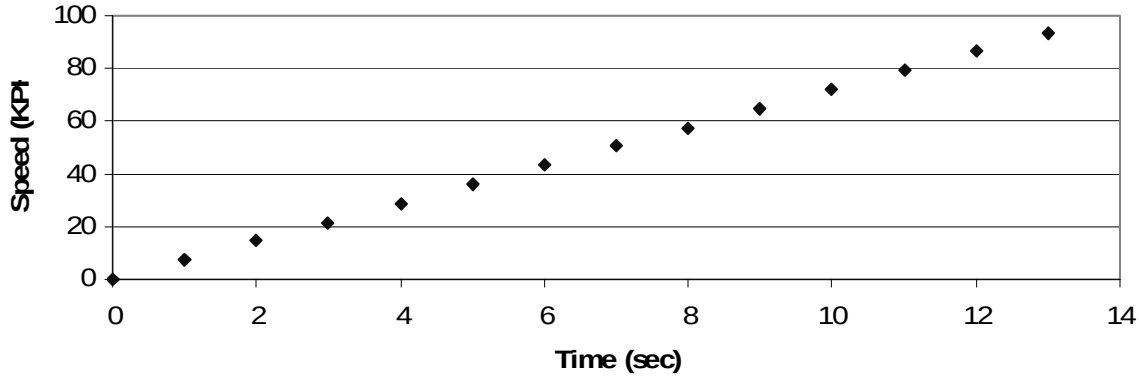

References

[1] United States Department of Energy Efficiency and Renewable Energy. “Hydrogen, Fuel Cells, and Infrastructure Technologies Program: Multi-Year Research, Development and Demonstration Plan”, January 2005.

[2] United States Department of Energy Energy Efficiency and Renewable Energy. “Hybrid vehicle comparisons”, http://www.fueleconomy.gov/feg/hybrid_sbs.shtml. Accessed Dec. 2006

[3] EG&G Services, Parsons, Inc. Science Applications International Corporation, October 2000. “Fuel Cell Handbook (5th Edition)”, U.S. Department of Energy, Office of Fossil Energy.

[4] Burns, Larry. Advanced Technology Briefing, North American International Auto Show 2005

[5] Cesiel, Douglas, et al. 2006. Development of a Steer-by-Wire system for the GM Sequel. SAE 2006-01-1173

[6] Johnson, Valerie H., 2000. HEV Control Strategy for Real-Time Optimization of Fuel Economy and Emmisions SAE 2000-01-153.

[7] Mali, Taylor J., 2006. Fuel Cell Hybrid Powertrain design approach for a 2005 Chevrolet Equinox. SAE 2006-01-0744.

[8] U.S. Department of Energy, ChallengeX Competition, www.challengex.org. Accessed Dec 2006

[9] University of Waterloo Alternative Fuels Team, www.uwaft.com. Accessed Dec 2006

[10] Samborsky Steven MASc Thesis. “Design Simulation of a Ultracapacitor-Based Hybrid Electric Vehicle”, Mechanical Engineering, University of Waterloo 2006

[11] U.S. Department of Energy, Energy Information Administration, 2005.
http://www.eia.doe.gov/emeu/aer/pdf/pages/sec5_56.pdf, Annual Energy Review

[12] Cavallo, Alfred J., Hubbert’s Petroleum Production Model: An Evaluation and Implications for World Oil Production Forecasts, Natural Resources Research,Vol. 13,No. 4, December 2004

[13] Elizabeth A. Lowery (GM Vice President, Environment and Energy)
http://fastlane.gmblogs.com/archives/2005/11/, Accessed December 2006.

Graphic from : Mali, Taylor J., Keynote presentation Combustion Institute, Canadian Section, Spring Technical Meeting, University of Waterloo. May 14th – May 17th 2006.

[14] Musil, David. March 2006. Fuel Cells – Current Status and Prospects for the Future, Ballard Power Systems

[15] Energy Information Administration (Hybrid vehicle Statistics)
http://www.eia.doe.gov/cneaf/alternate/page/datatables/atf14-20_05.html. Accessed December 2005

[16] Heffner, Reid R. 2005. Effects of Vehicle image in Gasoline Hybrid Electric Vehicles, Institute of Transportation Studies. UCD-ITS-RR-05-08.

[17] Ogden, Joan M. 2004. Societal lifecycle costs of cars with alternative fuels/engines., Energy Policy 32, 7-27

[18] Images from: Mali, Taylor J., March 31st 2006. Automotive Simulation, Design and Optimization – A Capability Review. Pollution Probe, Toronto Canada

[19] Certification Division, Office of Mobile Sources, U.S. Environmental Protection Agency. 1993. Federal Test Procedure Review Project: Preliminary Technical Report. EPA 420-R-93-007

20 U.S. Environmental Protection Agency, 1980. Passenger Car Fuel Economy: EPA and 42 Road." Report No. EPA 460/3-80-010, September 1980, p.119.

[21] M.B. Stevens, 2006, Fuel Cell Hybrid Control Strategy Development. SAE 2006-01-0214

[22] Gaines, Linda, Cuenca, Roy. 2000. Costs of Lithium Ion Batteries for Electric Vehicles

[23] Image taken from BP hydrogen marketing brochure. http://www.bp.com/liveassets/bp_internet/globalbp/STAGING/global_assets/downloads/H/hydrogen_Fuel_Cells_insert_FINAL.pdf Accessed December 2006

[24] Andreas Zuttel, March 17th, 2004. Hydrogen Storage Methods, Published online: 17 March 2004 Springer-Verlag

[25] Bosco, Andrew (Manager, GM Fuel Cell Stack Research). HyWire Technical design, Presented at the Alternative Power Simulation Workshop, Herndon, VA. October 14th 2003.

[26] Image from Car Design online: http://www.cardesignonline.com/technology/necar-fuel-cell.php. Accessed December 2006.

[27] Honda, December 2004. Honda Fuel Cell Power (FCX) Press Information.

[28] Fuel Cell Works Supplement, March 2005. The Future of Fuel Cells (Source: Electrical Construction and Maintenance). http://www.fuelcellsworks.com/Supppage2203.html. Accessed December 2006

[29] Fuel Cells 2000. Technical Info - Transportation Fuel Cells. http://www.fuelcells.org/info/charts/carchart.pdf accessed December 2006

[30] HYPM 65 information: http://www.hydrogenics.com/power/pdf/HyPM_HD-XR_Brochure.pdf Accessed December 2006

[31] ZM180 reference: http://www.dynetek.com/pdf/350_Bar_Specifications.pdf. Accessed December 2006

[32] DC/DC converter design: Jen Marshall, Electrical Engineering, University of Waterloo

[33] Ballard motor: http://www.ballard.com/resources/transportation/ballardedpc312v67ms.pdf Accessed December 2006

[34] Cobasys 288-60: http://www.cobasys.com/solutions/transportation.htm. Accessed December 2006

[35] Mali, Taylor J., Keynote presentation Combustion Institute, Canadian Section, Spring Technical Meeting, University of Waterloo. May 14th – May 17th 2006.

[36] Stevens, B, Mathew 2005.Optimization of a Fuel Cell Powertrain for a Sport Utility Vehicle, International Green Energy Conference, University of Waterloo.

[37] NEC Corporation Nov 2002. An Introduction to Vector Control of AC Motor using the V850. Document No. U16483EE1V0AN00

[38] Dave Barthmuss (GM Communications GM fastlane blog) http://www.gm.com/company/onlygm/fastlane_Blog.html#EV1 Accessed December 2006

[39] California Air Resource Board website, http://www.arb.ca.gov/homepage.htm. Accessed December 2006

[40] CARB meeting minutes, Friday March 28th, 2003. Transcripts provided by "Peters Shorthand Reporting Corporation"

[41] All motor efficiency data provided by Ballard Power Systems. Derek Mathews 2006, Customer Service and Application Engineering Manager

[42] www.ballard.com. Accessed December 2000.

[43] A.J. Pohlmeyer, 2005 (Sr. Field Application Engineer). Controller Area Network technical details presented at the Orlando Freescale Technology Forum 2005.

[44] OnStar system by GM. www.onstar.com. Accessed December 2006

[45] Mototron website: http://www.mototron.com/home.asp. Accessed December 2006

[46] MPC565 Automotive Controller by Freescale Semiconductor: http://www.freescale.com/webapp/sps/site/prod_summary.jsp?code=MPC565&nodeId=016246PCbf8648#links. Accessed December 2006

[47] The Mathworks (Simulink Developer): http://www.mathworks.com/ Accessed December 2006

[48] Greenhills embedded contoller development tools: http://www.ghs.com/ Accessed December 2006

[49] Morency, Kevin, et al., Using Graph Theory and Symbolic Computing to Generate Efficient Models for Vehicle Dynamics, Canadian Society for Mechanical Engineering Forum, Kananaskis, Alberta, 2006

[50] Mendes, Chris J., 2004. PSAT Model Verification of a Chevrolet Equinox. University of Waterloo Alternative Fuels Team

[51] EPA common drive cycles: http://www.epa.gov/otaq/labda.htm Accessed December 2006